Developing Lathing Parameters for PBX 9501

by

Randall Brock Woodrum, B.S.E.E.

A Thesis

in

Electrical Engineering

Submitted to the Graduate Faculty
of Texas Tech University in
Partial Fulfillment of
the Requirements for
the Degree of

MASTER OF SCIENCES

Approved

Dr. Andreas Neuber
Committee Chairman

Dr. James Dickens

Dr. Mark Sheridan
Dean of the Graduate School

August, 2017

ACKNOWLEDGMENTS

I would like to thank those who supported me through the process of obtaining my Masters degree. I first would like to thank all my colleagues in the pulsed power lab, in particular David Barnett for helping with the building and data gathering of my experimental setup, as well as the technicians and Barbra Beller for help with construction and purchasing of materials. I would also like to thank Nicholas Wilson and Ricardo Rodriguez for helping formulate my ideas into working products.

I would especially like thank my advisor Dr. Neuber for pushing me beyond my limits to not only achieve this degree, but also learn many valuable life experiences in the process.

Lastly, I would like to thank my parents who taught me that nothing gets accomplished without hard work and dedication, and my fiancee Nicole for her endless support and patience throughout this process.

TABLE OF CONTENTS

ABSTRACT

This thesis presents the work performed on lathing PBX 9501 to gather and analyze cutting force and temperature data during the machining process. This data will be used to decrease federal-regulation-constrained machining time of the high explosive PBX 9501. The effects of machining parameters depth of cut, surface feet per minute, and inches per revolution on cutting force and cutting interface were evaluated. Cutting tools of tip radius 0.005 -inches and 0.05 -inches were tested to determine what effect the tool shape had on the machining process as well. A consistently repeatable relationship of temperature to changing depth of cut and surface feet per minute is found, while only a weak dependence was found to changing inches per revolution. Results also show the relation of cutting force to depth of cut and inches per revolution, while weak dependence on SFM is found. Conclusions suggest rapid, shallow cuts optimize machining time for a billet of PBX 9501, while minimizing temperature increase and cutting force.

LIST OF TABLES

LIST OF FIGURES

CHAPTER 1
Introduction

The High Explosive (HE) machining safety standards for plastic bonded explosives (PBX) set by the Department of Energy (DOE) were developed decades ago dating back to the first explosives safety manual written in 1978 [6]. The current limitations make machining HE a lengthy process which is not ideal when trying to manufacture it into a shape usable for an explosive application. The work done for this thesis involves the machining of the HE PBX 9501, which will be described in more detail in later sections. Current standards do not allow for machining speeds greater than 213.2 surface feet per minute (SFM) or a chuck rotational speed greater than 525 RPM. The feed rate of the cutting tool also may not exceed 0.03937 inches per revolution (IPR) [1]. The safety limit for machining PBX 9501 is defined in Figure 1.1 below.

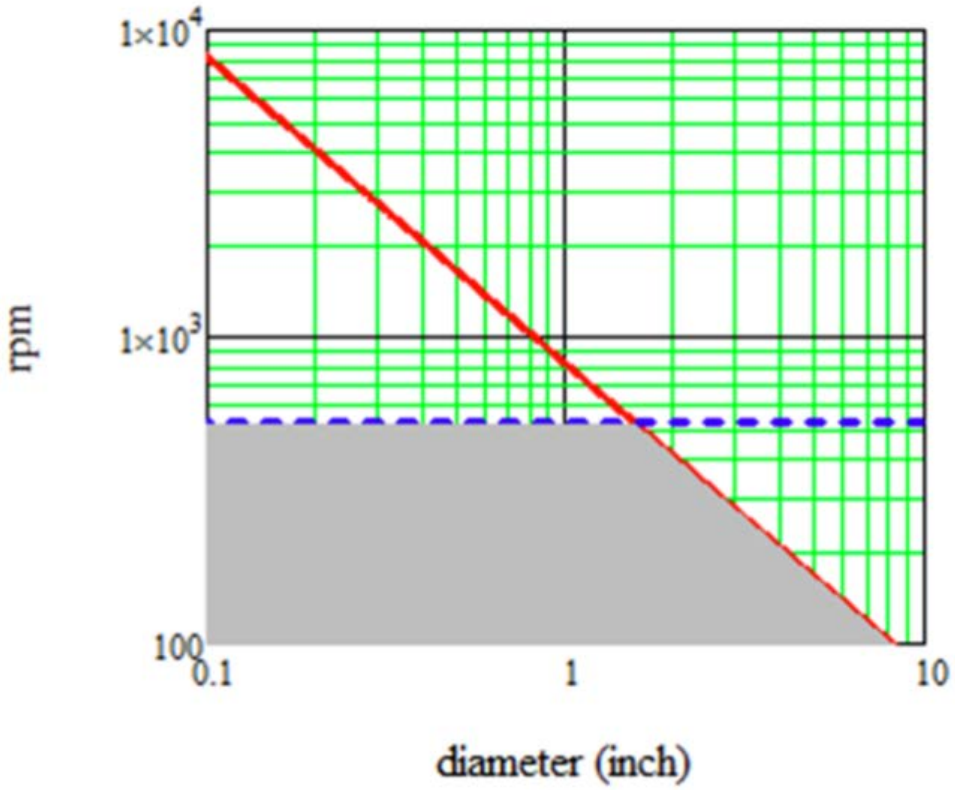

Figure 1.1. PBX 9501 Machining Safety Limit. SFM limit is represented by solid diagonal line and RPM limit is represented by dashed horizontal line. [1]

The area below the dashed line in Figure 1.1 is the zone in which the DOE considers safe to machine. This graph is a simplification of the DOE standards as it does not reference some parameters related to the machining process, such as IPR and DoC.

The purpose of this experiment is to test these limitations and push beyond the boundaries set by the DOE to formulate more accurate HE lathing safety limits. This is accomplished by measuring force and temperature during the machining process and evaluating when these parameters become too high for the HE to be machined safely. The parameters IPR, depth of cut (DoC), and SFM are varied between trials to better understand the effects of these parameters on the workpiece. The result of the experiment is to find the most effective combination of these parameters to give

the highest material removal rate (MRR) with force and temperature measurements within safe margins.

This thesis is divided up into two sections. The first section will cover the background, building, programming, and testing of the experimental setup. The second section will cover the gathered data, analysis, and observations taken from machining PBX 9501. A brief conclusion of the results and future work for this experiment will follow the second section for a look into the continuation of this experiment with other high explosive materials.

CHAPTER 2

Background

2.1 Lathe Machining

2.1.1 Initial Cutting Parameters

To better understand later topics discussed in this experiment it is important to understand the basics of lathe machining. The first topic to be discussed is initial cutting parameters. These parameters include feed rate, cutting depth, and cutting speed and are shown in Figure 2.1.

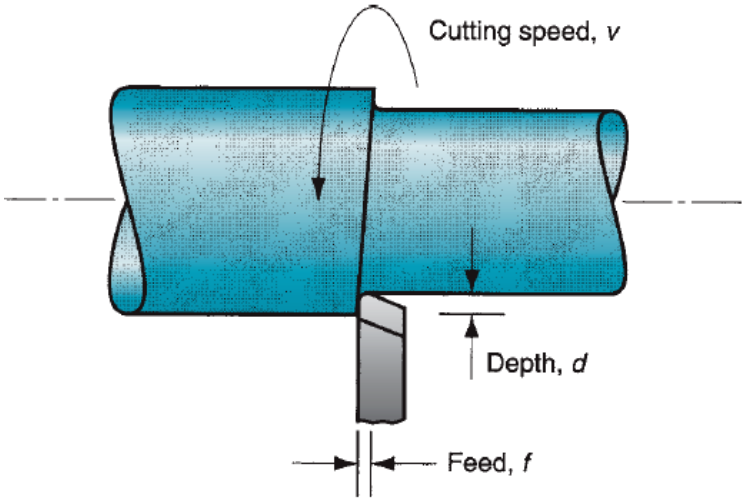

Figure 2.1. Cutting Parameters [2]

Feed rate is quantified by how many inches per minute (IPM) the cutting tool is traveling laterally down the workpiece. Slower feed rates allow for a smoother surface finish after a cut has been performed, though this limits the amount of material being removed per revolution of the workpiece. Depth refers to how much material is going to be removed from the workpieces in reference to the workpieces radius. This means twice the cutting depth will be removed from the diameter of the workpiece. It is important to keep in mind that most lathe encoders are programmed to show how much material is being removed from the diameter of the workpiece rather than the

cutting depth. Cutting speed is most commonly referred to as RPM and determines how fast the workpiece spins.

Varying these initial parameters will determine the speed, quality of finish, and heat generation/dissipation applied to both the cutting tool and the workpiece. These topics will be discussed in more detail in later sections.

2.1.2 Chip Formation

During the lathing process chips are shaved from the surface of the workpiece. The way a chip forms is dependent on the machining parameters, material of the workpiece, and the angle of the cutting tool shown below in Figure 2.2.

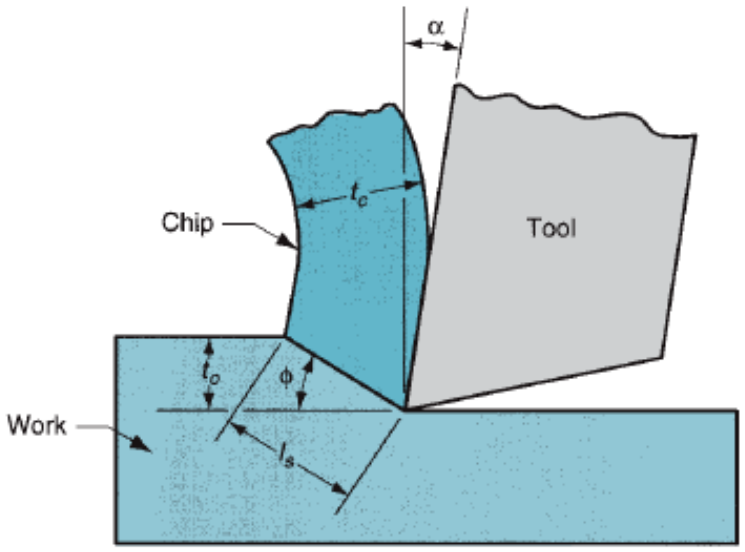

Figure 2.2. Chip Formation [2]

From the above figure, the thickness of the chip t_c is dependent on the relationship between the cutting depth t_o and the shear plane t_s formed by the cutting tool. The chip thickness expands as the shear plane becomes longer. This is an important concept for this experiment due to the thermal properties differently sized chips. When machining most metals in a lathe, the chip retains most of the heat formed during the cutting process due to the high thermal conductivity of the metal. During the experiment performed for this thesis the heat seemed to be distributed equally between the

cutting tool and the chip. PBX 9501 has mechanical and thermal properties closer to that of a chalk than a hard metal which could explain why the heat distribution is more uniform. Later sections will cover these results in more detail.

The two angles of importance to note from Figure 2.2 are the rake angle α and the shear angle ϕ. For this experiment, the rake angle was kept constant at 0 degrees which puts the cutting surface of the tool perpendicular to the workpiece. This was done to eliminate having to test an additional parameter due to the low number of PBX 9501 billets on hand. The shear angle is then dependent on the cutting and thrust forces which will be covered in the next section.

2.1.3 Forces Involved in Lathing Process

The three main forces that make up the cutting process are the cutting force (Fc), the thrust force (Ft), and the feed force (Ff). These forces are what is being measured during this experiment using a dynamometer to read the forces acting on the tool in the x, y, and z-axis. An orthogonal view of these forces are shown in Figure 2.3.

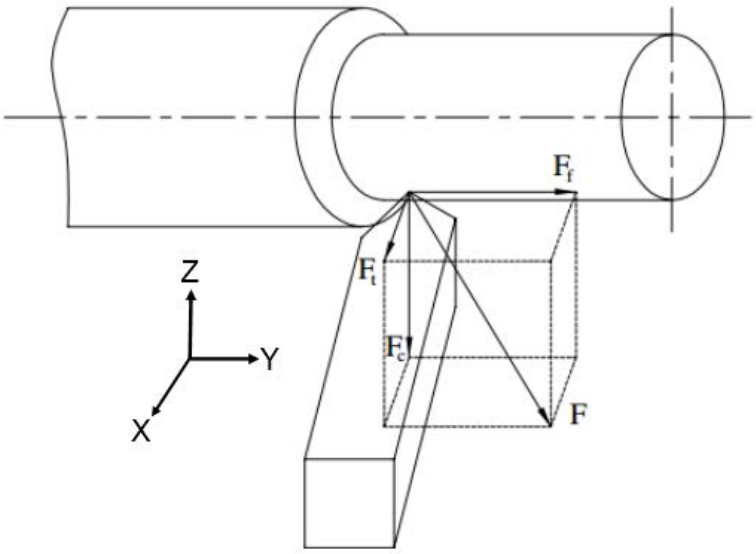

Figure 2.3. Forces Acting on Cutting Tool During The Machining Process [3]

The feed force is acting on the cutting tool in the lateral or x-direction of the workpiece while the thrust force is the force acting on the cutting tool in the radial

or y-direction. These two forces only make up a small part of the forces involved during the cutting process, although when attempting a large feed rate the feed force begins to make a larger contribution to the total force acting on the cutting tool. For most machining parameters however, the cutting force will contribute most of the force acting on the cutting tool. The cutting force is the force being applied in the downward or z-direction, which is the direction of cutting. As the cutting tool is introduced to the rotating workpiece the material is shaved off in the downward direction resulting in the force in the z-direction to be equivalent to the cutting force. For this experiment, we will mostly be observing the cutting force to define a safe margin.

2.2 Terminology

2.2.1 SFM, IPR, and DoC

Three abbreviations that are used very commonly throughout this thesis are SFM, IPR, and DoC. This section will briefly cover what parameters these terms correlate to and how they affect the machining process.

SFM refers to how many surface feet per minute the cutting tool is traveling along the surface of the workpiece. The equation for SFM is given by

$$SFM = \frac{RPM \cdot D \cdot \pi}{12} \tag{2.1}$$

In order to maintain a constant SFM during a lathing process, the RPM of the workpiece must be increased with each consecutive pass. This is due to the outside surface of the workpiece traveling faster than the inside of the workpiece, so as the diameter becomes smaller the RPM must be increased to keep the SFM constant. SFM for this experiment is typically within the range of hundreds to thousands of feet per minute.

The next topic will be IPR or inches per revolution and is defined as the amount of material in inches being taken off the workpiece by the cutting tool per revolution of the workpiece. IPR is calculated using the following equation

$$IPR = \frac{IPM}{RPM} \tag{2.2}$$

IPR directly correlates to the IPM the cutting tool is traveling across the workpiece and determines the quality of finish on the surface of the workpiece. The lower the IPR the smoother the finished surface of the workpiece will be. IPR for this experiment is typically measured in tens of mils.

The last topic discussed in this section is depth of cut, abbreviated as DoC. Depth of cut refers to how much material is going to be removed from the radius of the workpiece during one lateral pass of the cutting tool. The diameter being removed from the workpiece will be twice the depth of cut. The depth of cut has the largest impact on both force and temperature of all the other parameters. With an increase in DoC the resulting force and temperature will both increase causing more stress on both the cutting tool and the workpiece. For this experiment, the DoC ranged from 0.0625 in to 0.25 in.

To conduct this experiment DoC, SFM, and IPR were the 3 independent variables tested for. Other variables were not tested due to only having 8 billets of PBX 9501 to test. In order to accumulate enough data for an initial characterization the independent variables had to be limited. Another variable often tested is how cutter angle affects forces and heating during machining. This could be another potential variable to test in later experiments.

2.2.2 MRR

Material Removal Rate (MRR) is defined by how much material is being removed per second from the workpiece. For this experiment, MRR is calculated in $\frac{cm^3}{s}$ using the following equation

$$MRR = SFM \cdot IPR \cdot DoC \cdot 3.277 \tag{2.3}$$

MRR is a salient parameters of this experiment for decreasing the amount of time it takes to safely machine down a billet of HE. This is accomplished by using the combination of DoC, IPR, and SFM that will return a high MRR while minimizing cutting force and temperature during the cutting process.

2.3 High Explosive Machining

2.3.1 PBX 9501

High explosives are compounds that when ignited using a large shock will react rapidly at high temperature and pressure [7]. There are many different types of high explosives, however only PBX 9501 was tested during this experiment. This section will cover what PBX 9501 is and how it is manufactured.

PBX stands for plastic bonded explosive which means it is a high explosive chemical bonded together with a small amount of plastic for shaping. PBX 9501 is composed of 95% high melting explosive (HMX) and 2.5% polyurethane binder consisting of Estane and 2.5% plasticizer BDNPA-F [8].

PBX is manufactured into billets using hydrostatic pressing by placing the explosive in a rubber bag and introducing it to a high-pressure water bath between 12,000 and 20,000 psi until it is dense enough to hold its shape [7]. The billet in its crude shape is hard to use in applications which is why it must then be machined down into a shape charge. There are problems that can occur during the manufacturing process that can be potentially dangerous during machining. Metal shavings could potentially be mixed in with the PBX during processing, and unless spotted on an x-ray the metal could spark during machining and set off the PBX. Another potential hazard formed during manufacturing are internal cracks inside of the explosive. These cracks could cause the explosive to break apart and be ejected away from the

bulk of the workpiece during machining. Another danger to watch for when working with PBX 9501 is the polymorphous transformation point of the explosive. After the explosive has undergone this transition it becomes less stable and is more susceptible to a reaction. The polymorph point for PBX 9501 is around 180 °C [4]. A study done on the phase transition from β to δ of PBX 9501 showed the temperature and how long the phase transition took to occur. Results from this study are shown below in Figure 2.4.

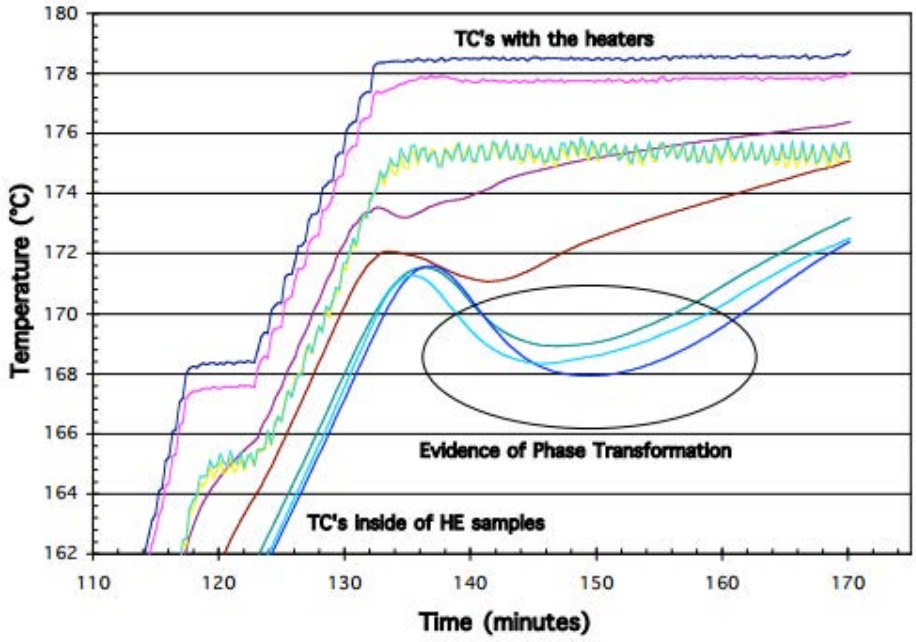

Figure 2.4. Phase Transition of PBX 9501 [4]

The circled zone in Figure 2.4 shows the thermocouple measured temperatures of the PBX while it is undergoing this phase transition. The phase transition can take anywhere from 30 minutes to an hour to complete once the polymorphic temperature has been reached.

The physical properties of PBX 9501 resemble that of a chalk or soft platic material. Some of these physical properties are compared below in Table 2.1.

Table 2.1. Comparison of Material Physical Properties

$Physical Property$	PBX 9501	Plexiglass	Chalk	Aluminum
$Physical\ Density\ (g/cm^3)$	1.843	1.18	1.442	2.7
$Specific\ Heat\ (J/g*K)$	1.13	1.465	0.9	0.9
$Thermal\ Conductivity\ (W/m*K)$	0.451	0.562	0.09	237
$Tensile\ Strength\ (MPa)$	9.24	68.948	0.23	310

By comparing the results in the table it is clear that PBX 9501 resembles material properties between a chalk and a plastic, but its properties are much different than that of a soft metal such as aluminum.

2.3.2 Other Experiments Involving PBX Machining

In 1988, engineers at Pantex did an investigation into the forces acting on a cutting tool when lathing several high explosive materials including PBX 9501. The experiment analyzed which parameters affected the x, y, and z force components to better enhance safety when lathing high explosives. The experiment consisted of a three-axis transducer that measured the each force component while sweeping through a range of different IPR, DoC, and cutting tool angle values. Three different cutting tools were used, each with a different cutter radius. The results of the experiment found that the DoC and IPR have the most effect in the x-direction correlating to the feed force while the thrust force in the y-direction was mostly affected by the angle of the cutting tool α. The cutting force in the z-direction seemed to be affected most by a change in DoC, resulting in a significant change in force acting on the cutting tool which can be seen in Figures 2.5 through 2.7 [5]. The following figures show the results of this data using a 0.05 inch radius cutting tool.

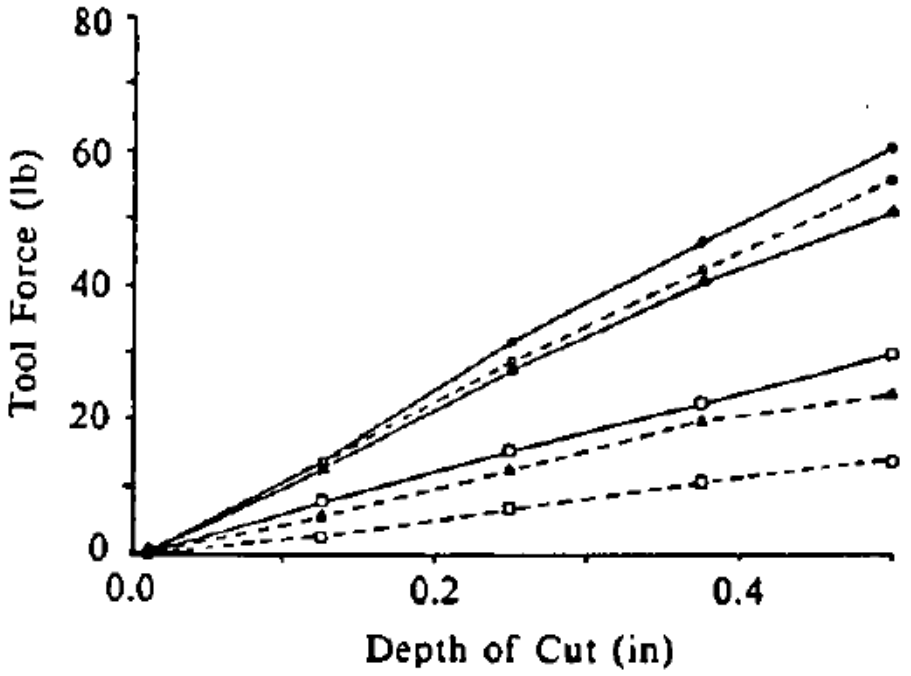

Figure 2.5. X-Component of Force for PBX 9501. Depth of Cut is defined as the amount of material removed from the diameter of the workpiece (for this figure only). Solid lines represent a cutter angle of 45° while solid lines represent a cutter angle of 90°. Three feed rates measured in IPR were used for each cutter angle and are indicated by squares (0.010), triangles (0.020), and circles (0.035) [5]

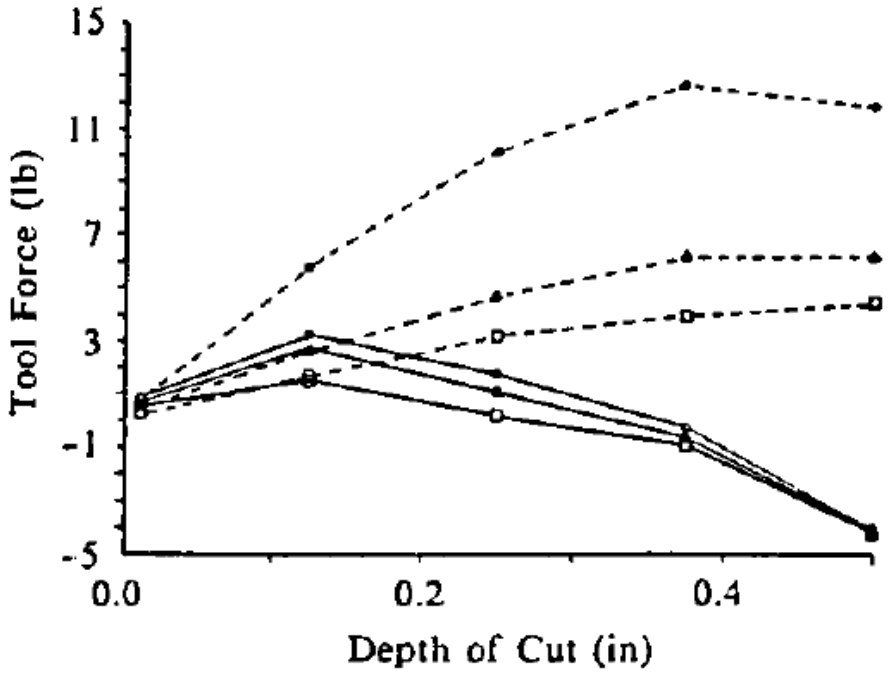

Figure 2.6. Same as Figure 2.5, Y-Component of Force [5]

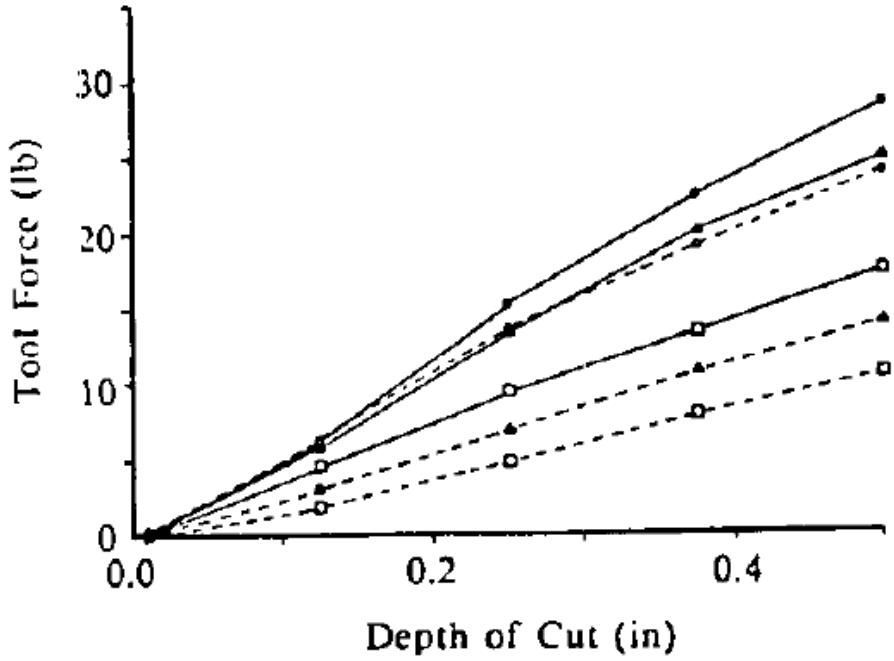

Figure 2.7. Same as Figure 2.5, Z-Component of Force [5]

The above figures represent different feed rates using a square (0.01 inches), triangle (0.02 inches), and a circle (0.035 inches). The different rake angles shown are represented with solid (45°) or dashed (90°) lines. From these graphs it can be concluded that x-components are most affected by DoC and IPR, y-components are most affected by rake angle, and z-components are affected by all three of the changing parameters.

Another paper published in China in 2005 investigated the effects of machining parameters on cutting forces and temperatures while lathing PBX. This experiment used a similar setup to the Pantex experiment by using a three-axis dynamometer to measure forces, while also incorporating a thin-film thermocouple onto the cutting tools surface to measure the temperature of the cutting tool. While the two experiments were very similar, this paper showed conflicting results. It concluded that the main cutting force in the z-direction was much less than forces in the x and y-directions, though the tests were performed the same way [9].

The experiment performed in this thesis resembles trends closely matching the work done at Pantex as opposed to the work done in China which will be described in later sections.

CHAPTER 3

Experimental Setup

The experiment designed to test the PBX 9501 consists of a remote operated manual lathe utilizing a dynamometer to test for forces associated with the lathing process, as well as thermocouples to test for the temperature of the cutting tool. The manual lathe had to be outfitted with stepper motors and controlled using an FPGA. Figure 3.1 shows an overhead view of the experimental setup.

Figure 3.1. Overhead View of Experimental Setup

Figure 3.2 pictured below represents the experimental setup used for this work.

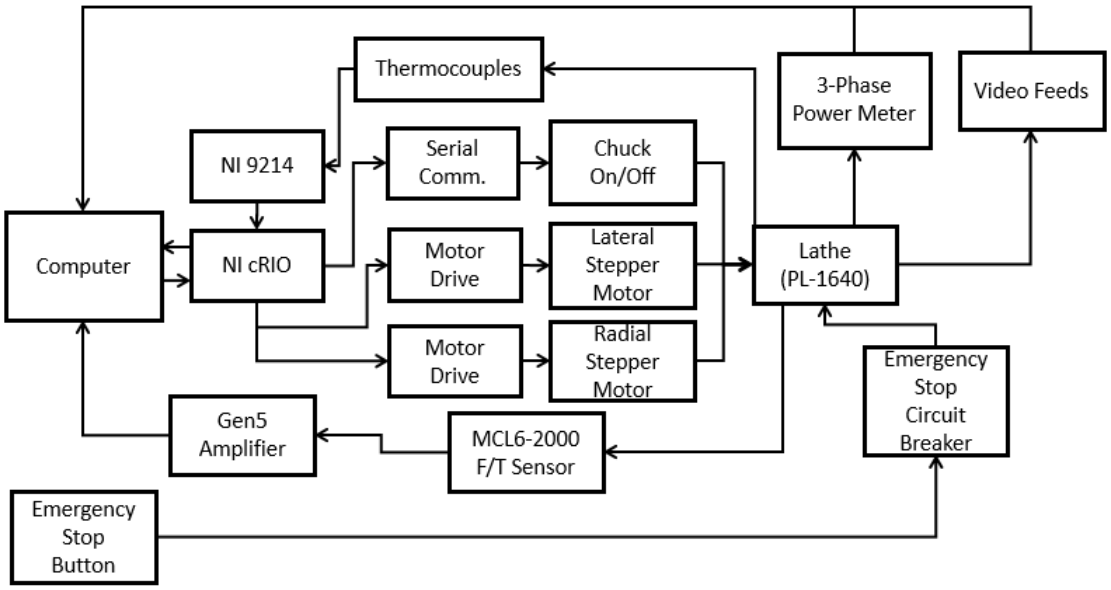

Figure 3.2. Experimental Setup Block Diagram

The following sections describe each block of the diagram in more detail.

3.1 Lathe Components

3.1.1 Lathe

One of the first decision to be made for the experimental setup of this project was what kind of lathe to buy. The limiting factor was space to be occupied by the lathe. The previously constructed blockhouse the experiment was to be tested in is approximately a 14 x 10 x 8 ft room. Because of the space constraint, it was much more cost effective to automate a manual lathe rather than buy a CNC lathe compact enough to fit the space.

The lathe used in this experiment was a Baleigh Industrial PL-1640 precision lathe shown in Figure 3.3.

Figure 3.3. Baleigh Industrial PL-1640 Precision Lathe

The specifications for this lathe are a 16 inch swing, which refers to the maximum diameter of the workpiece it can turn, and a 40 inch distance between centers referring to the maximum length of the workpiece it can turn. These dimensions allowed for plenty of room to attach other pieces of equipment to the lathe without interfering with the machining process. The specification for horse power was calcuated from the Pantex and Chinese experiments, mentioned in the background section of this thesis, using the following equation with a constant SFM of 1500.

$$HP = Cutting\ Force \cdot SFM \tag{3.1}$$

The maximum horse power required per the Pantex document was 0.789 HP [5], while the Chinese paper required 2.555 HP based on their maximum force measured, and our expected highest SFM of 1500 [9]. The lathe used in this experiment has a rating of 7.5 HP, which is more than enough to satisfy the requirement calculated in previous experiments.

The maximum RPM the lathe can supply is 2000, which is almost 4 times more than the current safety limitation. The last feature was a Mitutoyo position encoder integrated with the lathe shown below in Figure 3.4.

Figure 3.4. Mitutoyo Position Encoder

The encoder measures the distance the tool travels in both the lateral and radial directions. It is capable of measuring down to half of a mil and can output position data through an RS-232 port.

A concern with using a manual lathe for this experiment was the ability to operate the lathe remotely while machining the PBX. The lathe was rewired for remote on/off functions, as well as partially dismantled to allow for project adaptations [10]. These adaptations were accomplished using the system described in the next few sections.

3.1.2 Stepper Motors and Drivers

To control the longitudinal and radial movement of the cutting tool, the handles on the saddle of the lathe had to be replaced with stepper motors. The stepper motors allow for smooth motion throughout the machining process with precise start- and stop-points.

The stepper motors used for this experiment were NEMA 24 stepper motors capable of producing up to 380 oz-in of torque shown in Figure 3.5. The stepper motors lacked a sufficient amount of torque to turn the shafts controlling movement on the lathe, so gears had to be implemented to step up the torque supplied by the motors. A gearing ratio of 1:6.4 was used which provided more than enough torque to turn the shafts. While this sacrificed some speed provided by the stepper motors, their 3,000

RPM maximum rotation speed was capable of moving the lathe saddle at speeds of up to 40 IPM.

Figure 3.5. NEMA 24 Stepper Motors

In order to control the stepper motors, stepper drives had to be integrated into the setup as well. The drives chosen were Automation Direct STP-DRV-4850 advanced micro-stepping drives pictured in Figure 3.6.

Figure 3.6. STP-DRV-4850 Stepper Motor Drive

The drives can supply up to 5 A per phase and 24 to 48 VDC to the motor they are controlling. The drivers can step a motor from 200 up to 51,200 steps per revolution for applications that require high precision such as the work done for this experiment. The drive comes equipped with an RJ11 port for serial communication using RS-232

protocol from an FPGA or microcontroller. The stepper drives were controlled using an FPGA that will be described in later sections.

3.1.3 Force/Torque Dynamometer

A critical part of the experiment was obtaining a sensor to measure the x-, y-, and z-directional forces acting on the cutting tool during the machining process. This was accomplished by using AMTIs MCL6-2000 lathe dynamometer shown in Figure 3.7.

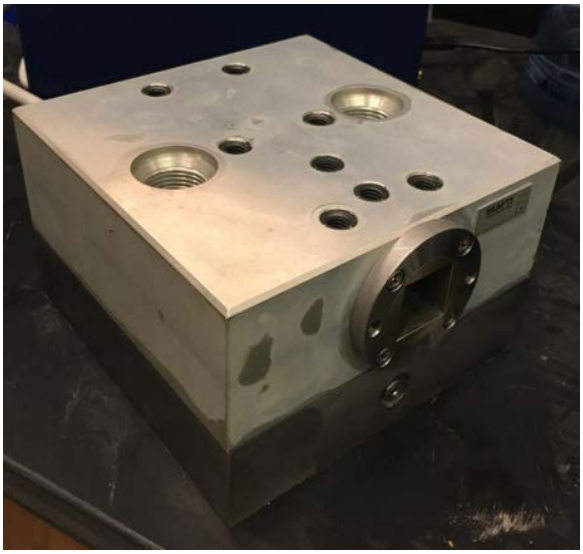

Figure 3.7. AMTI MCL6-2000 Dynamometer

This dynamometer is capable of measuring forces in the x-, y-, and z-directions as well as the moments around them. It can measure up 8.9 kN of force in the direction of the main cutting force and is accurate down to 0.5 N. The saddle on the lathe was stripped of all tool mounting components and the dynamometer was mounted onto the saddle in their place. The adapter mounting the dynamometer to the lathe saddle can be rotated a full 360 degrees to achieve any cutting angle, should the experiment require it. A drawing of this adapeter is shown in Figure 3.8.

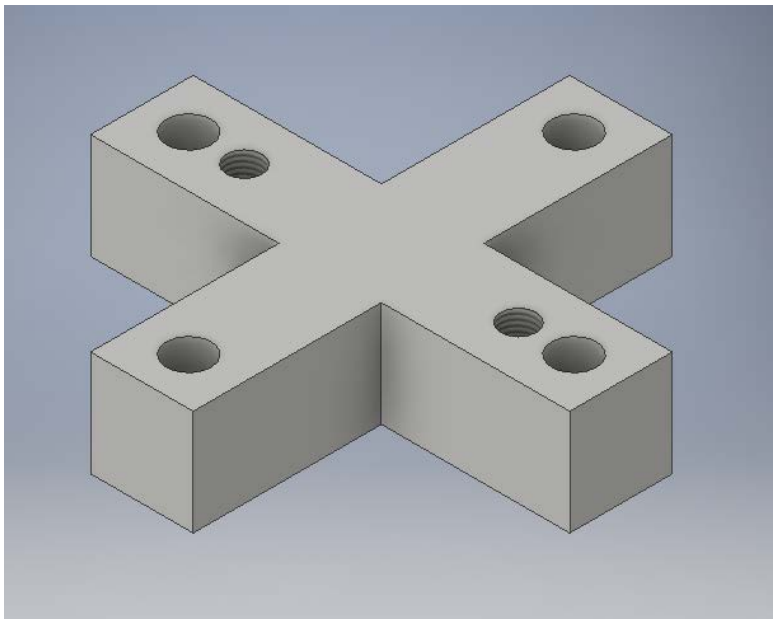

Figure 3.8. Drawing of Dynamometer Mount

Lastly, the cutting tool was mounted into a 1 x 1 in adapter and inserted into the tool slot on the sensor and bolted into place. The drawing for this adapter is shown below in Figure 3.9.

Figure 3.9. Cutting Tool Adapter

The dynamometer uses a transducer to measure when a force is applied to the sensor. The applied force changes the resistance of a variable resistor which can

then be measured as a voltage by the transducer. These voltages must then pass through an external amplifier before being transmitted via USB to the computer for analysis. The amplifier that was shipped with the sensor was a Gen-5 digital signal conditioning amplifier. This amplifier was a recommended accessory to the sensor and already came equipped with the 26-pin D type input for communication with the sensor. There were several issues with noise when using this sensor. The first was interference between the cable containing the sensor readings and other power cables at higher voltages coupling into the signal cable. To solve this problem the signal cable had to be run separate from all other cables to limit the noise picked up. Another noise problem in the sensor was generated from the stepper motor vibrations. These vibrations caused a slight ripple in the readings that was filtered out in post processing. The dynamometer interfaces through a software called NetForce which will be described in more detail in later sections.

3.1.4 Variable Frequency Drive

As described in an earlier section, to maintain a constant SFM during a machining process, the RPM of the workpiece must be increased as material is shaved off the diameter. This concept, along with the manual lathe chosen for this project only having 12 set RPM values to choose from, made a variable frequency drive (VFD) a necessity. A VFD is programmable controller that when interfaced with a motor can control the RPM based on varying the frequency and voltage at which the motor runs. By manipulating these parameters, the lathe could now run at any frequency between 0 to 2,000 RPM.

The VFD chosen for this experiment was a DURApulse GS3-27P5 pictured below in Figure 3.10.

Figure 3.10. DURApulse GS3-27P5 Variable Frequency Drive

This VFD has a horse power rating of 7.5 with a 3-phase input to match the PL-1640 lathe motor specifications. It uses a programmable logic controller to control the motor that can either be programmed manually, or remotely using an RS-485 (Modbus) protocol. The VFD was integrated into the lathe motor and controlled over RS-485 using an NI cRIO FPGA [11]. The control process will be described in later sections.

3.1.5 3-Phase Power Meter

To help verify force readings, the power going into the lathe was to be monitored and compared with the power going into the machining process. This required a 3-phase power meter that could measure the changes in power of the 3-phase input into the lathe before and after a billet is machined. The Simpson AMIK 201 digital power meter shown in Figure 3.11 was chosen for this measurement.

Figure 3.11. AMIK 201 Digital Power Meter

The AMIK 201 features 3 LED displays for quick measurement verification and can be used to measure voltage, current, or power quantities. It can also interface with controllers via RS-485 for setup and data logging applications. For this experiment, the power meter was interfaced over RS-485 with an NI cRIO FPGA. The data logging process will be covered in more detail in later sections.

3.1.6 NI cRIO FPGA

Operating the machining process remotely had to be accomplished by controlling all of the equipment above through a controller that could handle multiple processes simultaneously. For this reason, a field programmable gate array (FPGA) had to be used because of its ability to handle and process incoming data while controlling the motion of the stepper motors simultaneously.

The FPGA chosen for this project was a National Instruments compact reconfigurable input output controller (cRIO) 9074 shown below in Figure 3.12. This cRIO has a 400 MHz CPU and a 2M FPGA. The unique features of the cRIO is the plug-and-play design for modules specific to an application. Modules that were used in this experiment were RS-232 and RS-485 serial communication modules and a 16 channel thermocouple input module.

Figure 3.12. NI cRIO 9074

Serial communication modules were utilized to communicate with the stepper motor drives, VFD, and the 3-phase power meter. The two modules have 4 RJ50 ports and can support communication with up to 4 devices each.

A NI 9214 thermocouple module capable of sourcing measurements from up to 16 different thermocouples simultaneously was also used. It has a maximum sampling rate of 68 samples per second when all channels are in use, however it can sample faster when using fewer channels. In this experiment thermocouples are imbedded near the cutting edge of the tool as shown in Figure 3.13. The data is then sent to the thermocouple module and logged with the cRIO. This technique is used to gather cutting interface temperature data during the machining process.

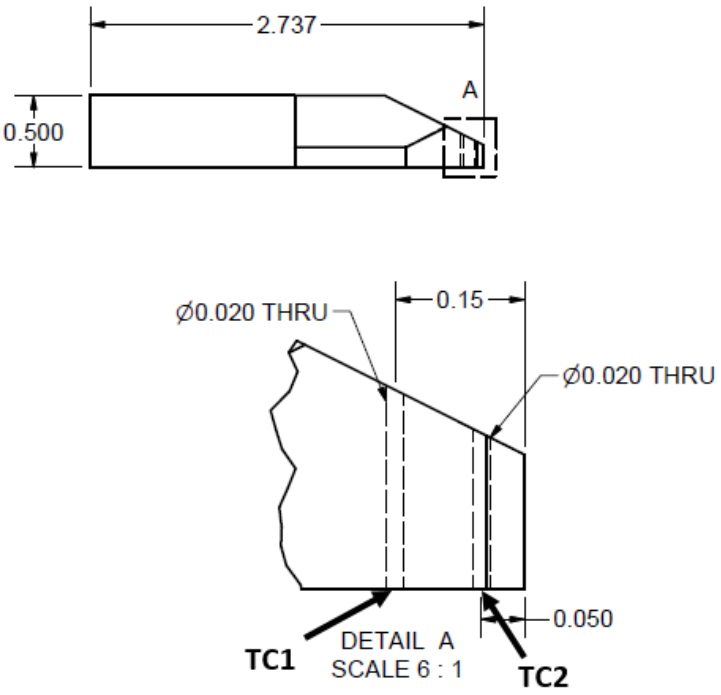

Figure 3.13. Omega 5TC-TT-K-36-36 Thermocouple Imbedding Drawing. TC1 and TC2 indicate thermocouple locations.

The cRIO is connected to a computer through a router network on an Ethernet port. It is controlled and programmed on the computer using National Instruments software LabVIEW, which will be explained in the following section.

3.2 Control Software

3.2.1 LabVIEW

LabVIEW is a graphical programming language developed by National Instruments. For this work, it was used to control the cRIO by providing an interactive user interface panel shown in Figure 3.14.

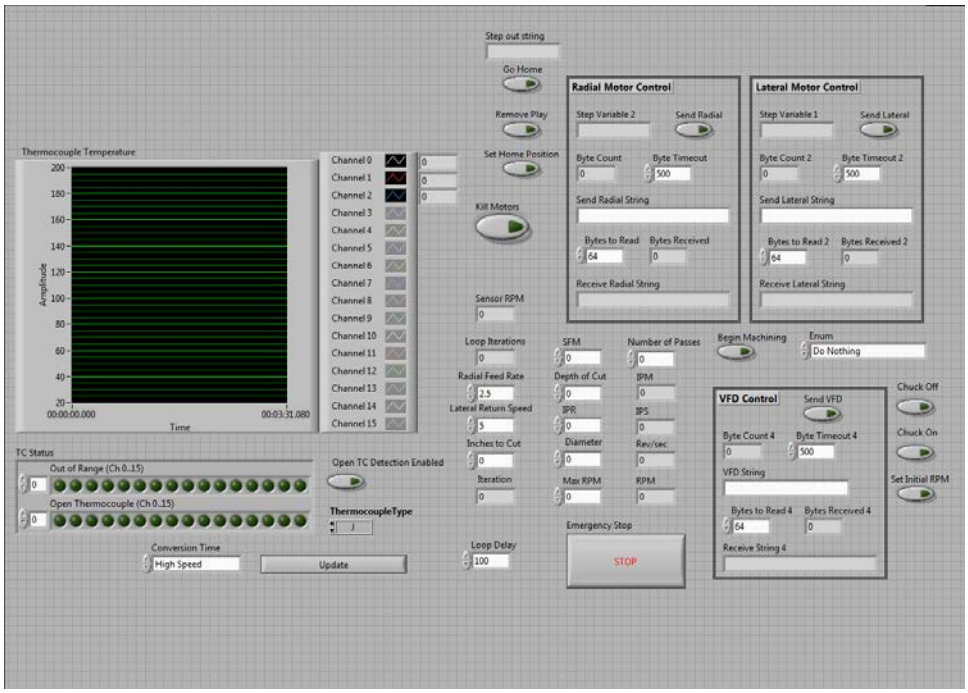

Figure 3.14. LabVIEW Automated Machining Front Panel

The user interface is divided up between multiple functions. The graph on the left side of the panel displays the measured thermocouple temperatures in real-time throughout the machining process. To the right of the graph are controls for manually jogging and resetting the stepper motors attached to the lathe. The lower right corner of the panel is for on/off functions, as well as manually setting and updating the chuck on the lathe. The last section in the middle of the panel is for inputting initial machining parameters such as SFM and IPR before executing a pass. The Begin Lathing Operation button located in this section will begin the automated machining process, as specified by the initial machining parameters, for the specified number of passes.

Running behind the user interface is the code for the LabVIEW program. It is programmed using a flowchart based approach where code is executed from block to block following wires between the blocks. The code for the program in this experiment is divided into two sections. The FPGA program handles the FPGA controls while the top program interfaces the user functions between the computer and the FPGA.

The FPGA program is designed to execute multiple functions simultaneously. It then handles commands given to it by the top program as inputs and outputs between the computer and the cRIO modules. Screenshots of the detailed block diagrams used for the LabVIEW code can be found in appendix A.

Figure 3.15 shows the simplified flowchart for how the automated machining process executes once the Begin Lathing Operation button has been pressed. A more detailed flowchart for this process can be found in appendix A.

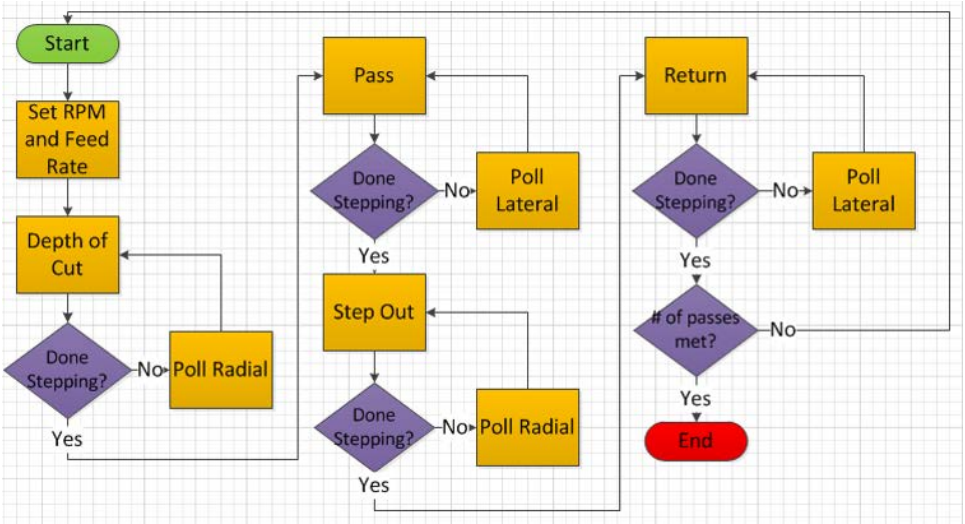

Figure 3.15. Simplified Flowchart for Automated Machining Process

The program first sets the stepper motors velocities based on the specified input parameters. A radial position is then given to motor 1 to position the tool to the depth of cut. A lateral position is then given to motor 2 to execute the cut along the workpiece. The motors are then ordered back to their original positions, and if another pass is specified the program executes again and moves the radial position to the depth of cut times the current pass.

3.2.2 NetForce

NetForce is the software used with the dynamometer for logging the force and torque data collected by the sensor. The user interface, shown in Figure 3.16, displays

force readings in the x-, y-, and z-directions in the top left graph, while displaying torque readings in the bottom left graph.

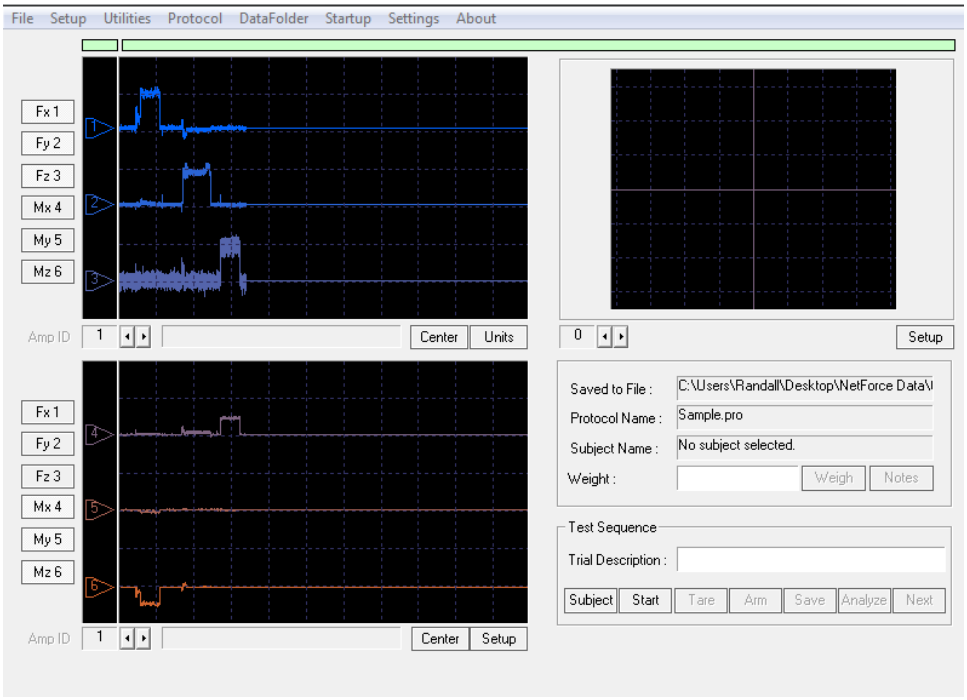

Figure 3.16. NetForce User Interface

Once a set of data has been gathered, NetForce has the ability to export all six sensor readings in a .csv file to be used in spreadsheet based graphing software. Some functions such as zeroing the sensor and starting or stopping sampling can also be handled through the user interface.

3.2.3 Blue Iris

In order to observe what is happening inside the blockhouse during a machining run, two cameras were set up for multiple views of the process. These cameras were controlled through a software called Blue Iris. Blue Iris has the ability to display multiple videos feeds for simultaneous viewing. It can take advantage of pan/tilt/zoom (PTZ) camera functions as well. The user interface for Blue Iris is pictured below in Figure 3.17.

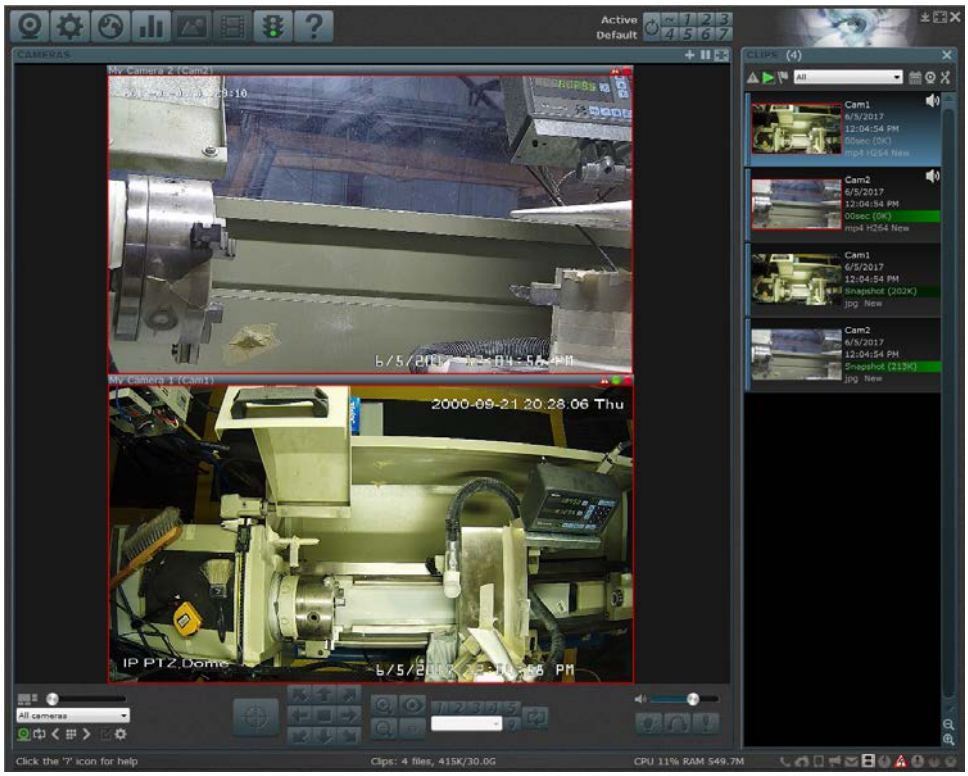

Figure 3.17. Blue Iris User Interface

For reviewing purposes, the video footage of the machining process also had to be recorded. This software allows for a motion activated trigger to begin video recording or a manual trigger within the program. For this experiment, a manual trigger was set and began recording on both cameras once triggered while also taking snapshots every 30 seconds. Blue Iris allows for videos and snapshots to be exported from the program as any video or picture format for viewing through other programs.

CHAPTER 4

Experimental Results and Analysis

The results of this work will be used to decrease the amount of time it takes to safely machine a billet of PBX 9501. In order to achieve this, the machining safety boundaries defined by the DOE had to be far exceeded. Figure 4.1 shows the data points where each pass occurred on the machining safety limit graph.

Figure 4.1. Experimental Machining Points in Reference to Safety Limit for PBX 9501

4.1 Temperature Analysis

Temperature was one of the two main quantities measured during this experiment. It is important to measure temperature during this process to try and avoid the polymorphic temperature of PBX 9501 which is approximately 180 °C [4]. At this temperature, the PBX begins to become more unstable while being machined, and a reaction is more likely to occur.

Ideally the temperature of the tool at the cutting interface would like to have been observed, however it proved very difficult to obtain this data. An article written 2007 described many different approaches to accomplishing this temperature measurement

while machining [12]. Several approaches were considered such as IR video capture, thermocouple imbedding, and layering a thermocouple on the surface of the tool. It was decided the best approach would be to embed thermocouples into the tool tip, as described in section 3.1.6, and compare experimental data with the simulated data. Figure 4.2 shown below is an example of one pass while machining PBX 9501.

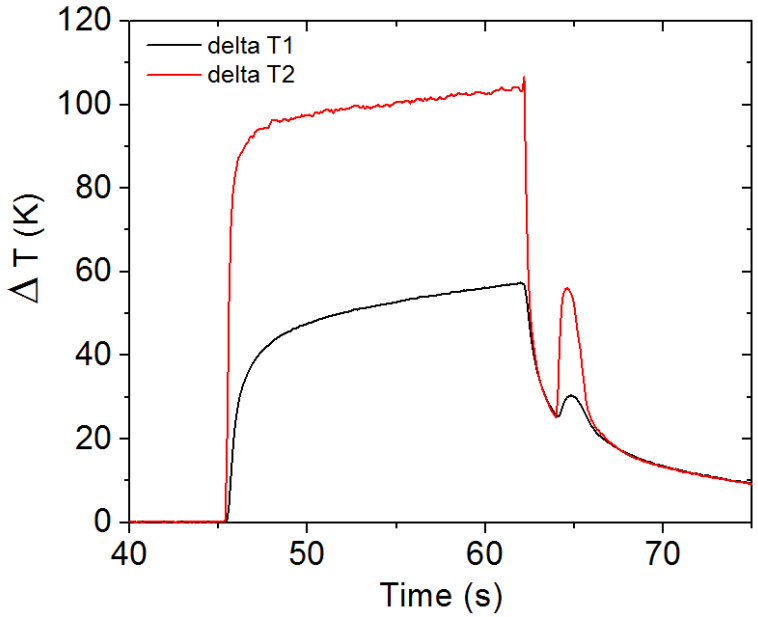

Figure 4.2. Billet 4 Trial 3 Temperature Measurements for 0.005" Tool. See Figure 3.13 for thermocouple locations.

Figure 4.2 shows the two different temperature readings from the testing done on billet 4 trial 3. One observes the thermocouple closest to the cutting interface (red) is much hotter than the other thermocouple even though they are only 0.1 inches apart. The small temperature peak at the end of the machining pass is due to facing the base of the billet once a pass has been completed.

The incorporation of an IR camera was used to gather evidence of how the heat is distributed between the tool and the chip. Figure 4.3 below shows an on-end view of the tool and chip during the machining process.

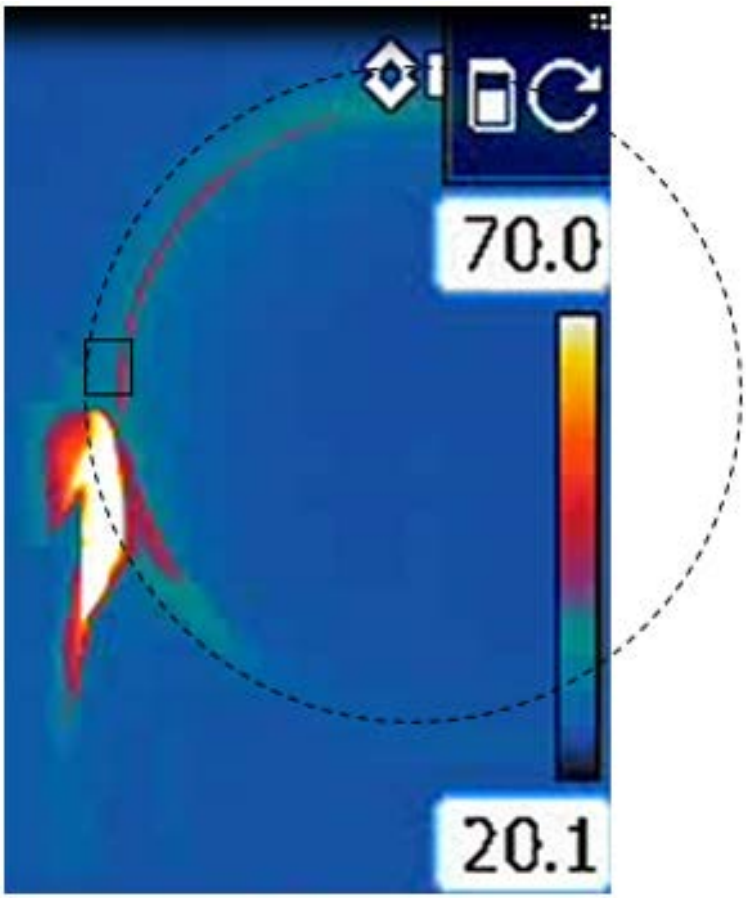

Figure 4.3. IR Snapshot of Machining Process

From the figure above the dashed line shows the workpiece diameter before the cut and the square shows the DoC. The figure shows the chip has majority of the heat associated with it leaving only a small amount of heat being absorbed into the workpiece. The cutting tool is hidden behind the chip in this image, however from what is visible the cutting tool also seems to be approximately the same temperature as the chip. Another aspect to note is the temperature gradient associated with the chip. The following figure shows a view of both sides of the chip as it spirals off of the workpiece.

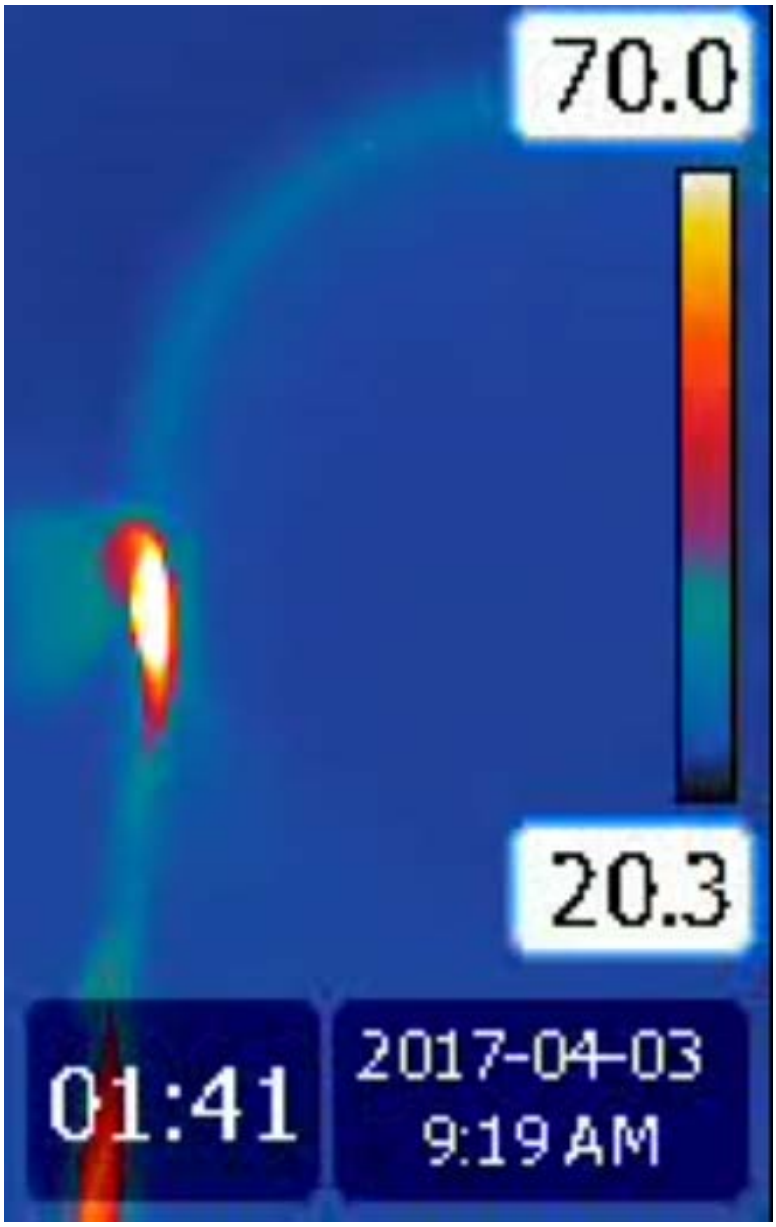

Figure 4.4. IR Snapshot of Ribbon Temperature Gradient

Figure 4.4 shows the temperatures of both sides of the chip. The temperature scale in this IR snapshot is fixed from 20.3 °C to 70 °C. The cutting tool at the cutting interface, and the side of the chip that faces the tool tend to have similar temperatures observed from IR and thermocouple data that has been collected during this experiment. From the data taken during this run, the cutting tool was measured to be 92.1 °C making the hotter side of the chip shown in Figure 4.4 approximately this value.

The cooler side of the chip looks to be around 30 °C making the temperature gradient between the two sides of the chip approximately 62 °C. This gradient increases with higher rates of removal such as an increased SFM or IPR, which also causes an increase in the temperature gradient between the two thermocouples imbedded in the cutting tool.

Two tools were used during this experiment, one with a 0.05-inch tip radius and another with a 0.005-inch tip radius. Temperature data using these two tools are shown in the following figures.

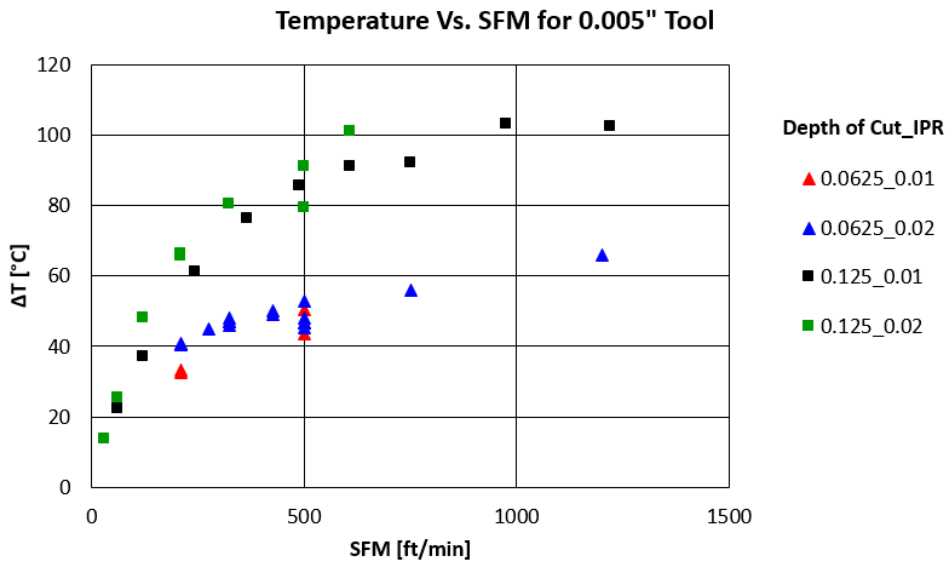

Figure 4.5. Temperature Vs. SFM for 0.005" Tool

Figure 4.5 shows the temperature trends for the 0.005-inch radius tool as SFM is increased while keeping DoC and IPR constant. Shapes denote the DoC while colors denote the IPR.

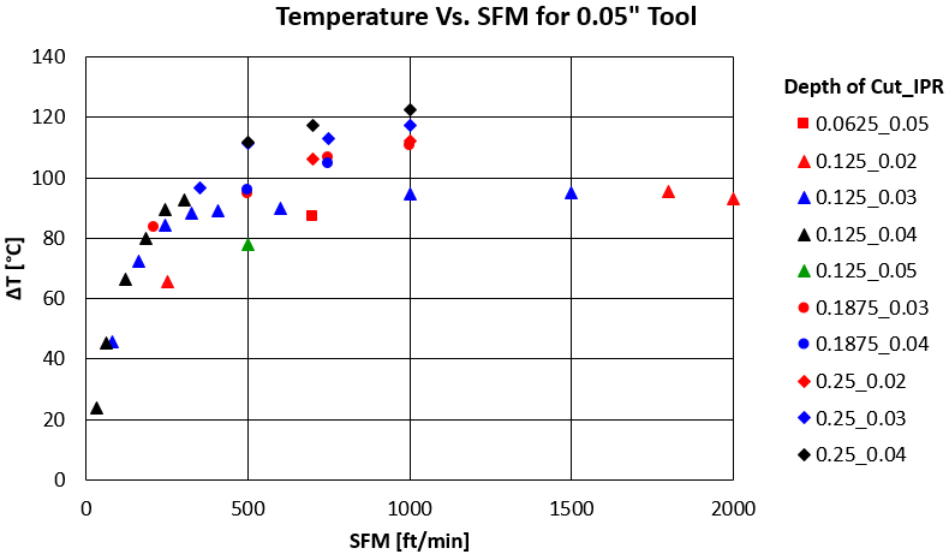

Figure 4.6. Temperature Vs. SFM for 0.05" Tool

Figure 4.6 shows the temperature trends for the 0.05-inch radius tool as SFM is increased while keeping DoC and IPR constant. Shapes denote the DoC while colors denote the IPR.

The data points represented on Figure 4.5 and 4.6 represent all the data taken while machining 8 billets of PBX 9501. The following observations can be realized by the above figures. An increase in SFM will lead to an increase in temperature. In addition to SFM, an increasing DoC also shows trends of temperature increase. The figures also show that varying IPR while keeping SFM and DoC constant do not result in a very large change in temperature. From these observations, it can be concluded that temperature during machining is sensitive to changes in both SFM and DoC, while less sensitive to changes in IPR. In addition to this data, the temperature at the cutting interface is expected to be 20 to 30 °C higher than the measured values due to the thermocouples not being exactly at the cutting interface.

A common function to describe cutting interface heating over time during lathe machining of metals is shown in equation 4.1 [2].

$$T = K \cdot v^m \tag{4.1}$$

In this equation T is the temperature of the cutting interface, v is the cutting speed, K is a constant as well as m and are dependent on material and other cutting conditions [2]. Examples of this equation were used in this work to describe the heating of the cutting tool versus the MRR and is shown in Figure 4.7.

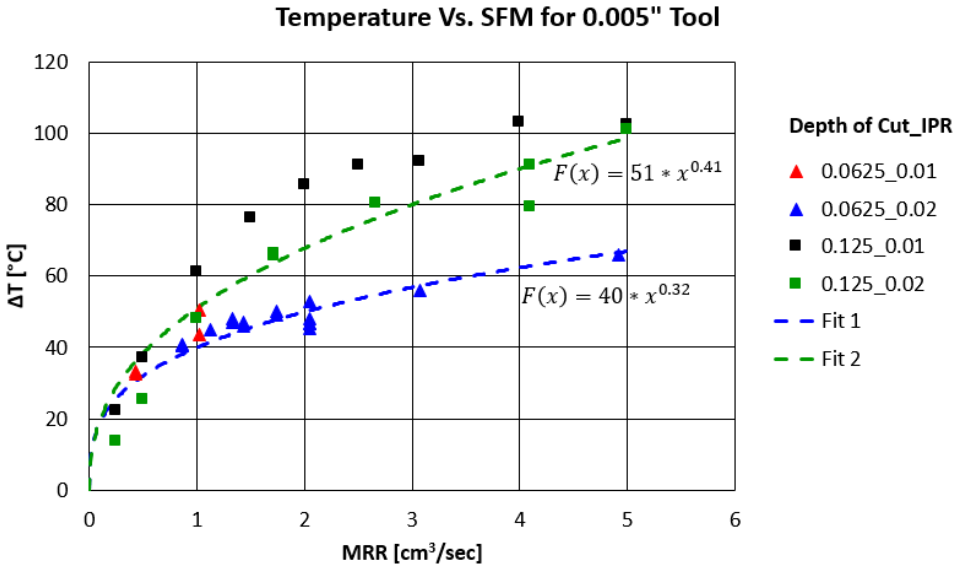

Figure 4.7. Temperature Vs. MRR for 0.005" Tool with Fitted Curves

The fitted curves in the above figure match up with equation 4.1 giving a general idea for how the heating of the interface will change as a function of cutting speed.

4.2 Force Analysis

The forces acting on the cutting during the machining process tool were the other main quantities this experiment was testing for. The three forces to be measured were the feed force, thrust force, and main cutting force. Though all three of these forces were measured, the cutting force in the z-direction was much higher during the machining process, leading to the results being analyzed against this factor.

To achieve these force readings the cutting tool was mounted into a dynamometer as described earlier in section 3.1.3. The data was then imported into OriginLab for postprocessing and smoothing. Figure 4.8 shown below is an example of one pass of data taken during the machining process after it has been postprocessed.

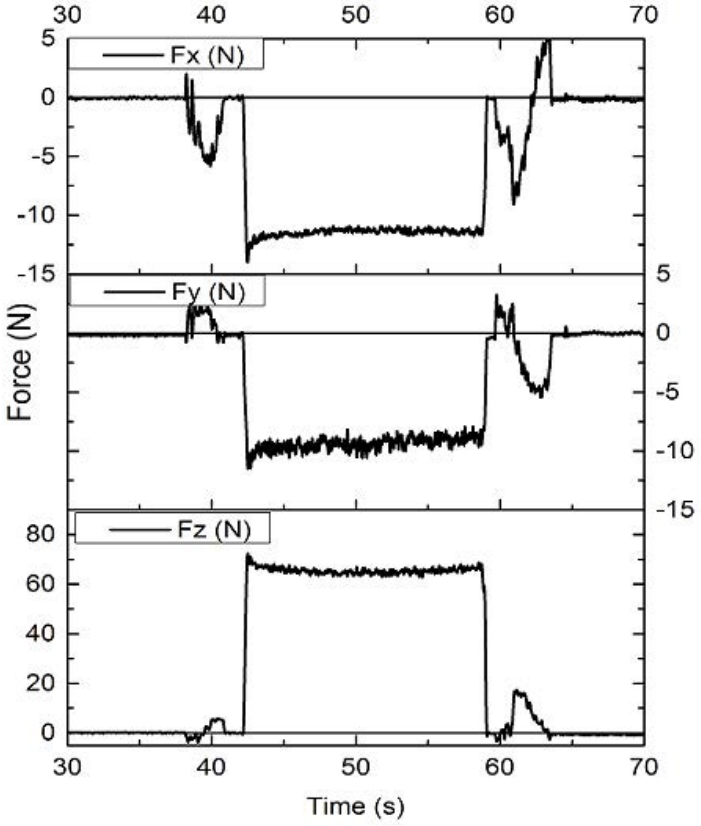

Figure 4.8. Billet 4 Trial 3 Force Measurements for 0.005" Tool

Figure 4.8 shows the forces recorded in the x-, y-, and z-directions during the experiment. The force recorded in the z-direction is the main cutting force. The average main cutting force during the cutting process was taken from this graph and used for the analysis in the following figures.

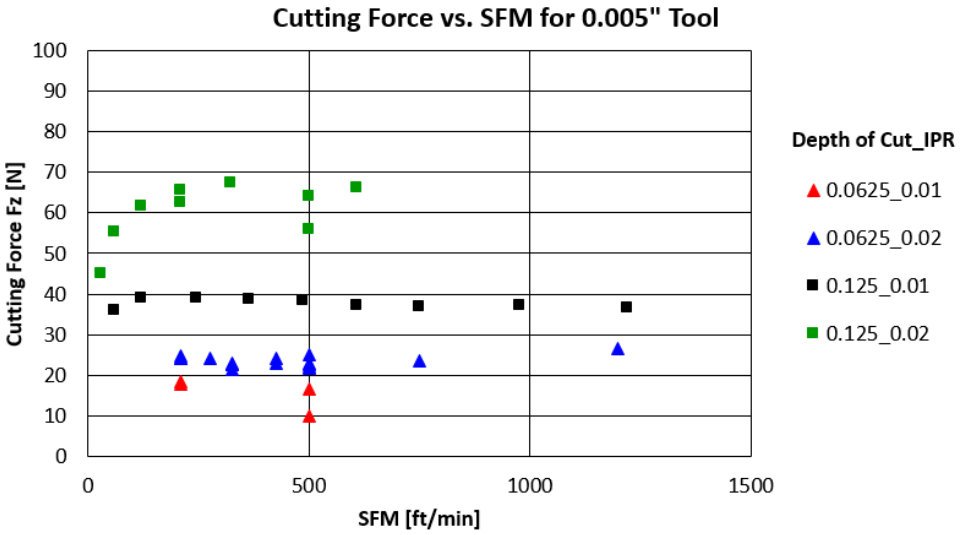

Figure 4.9. Cutting Force Vs. SFM for 0.005" Tool

Figure 4.9 shows the force trends for the 0.005-inch radius tool as SFM is increased while keeping DoC and IPR constant. Shapes denote the DoC while colors denote the IPR.

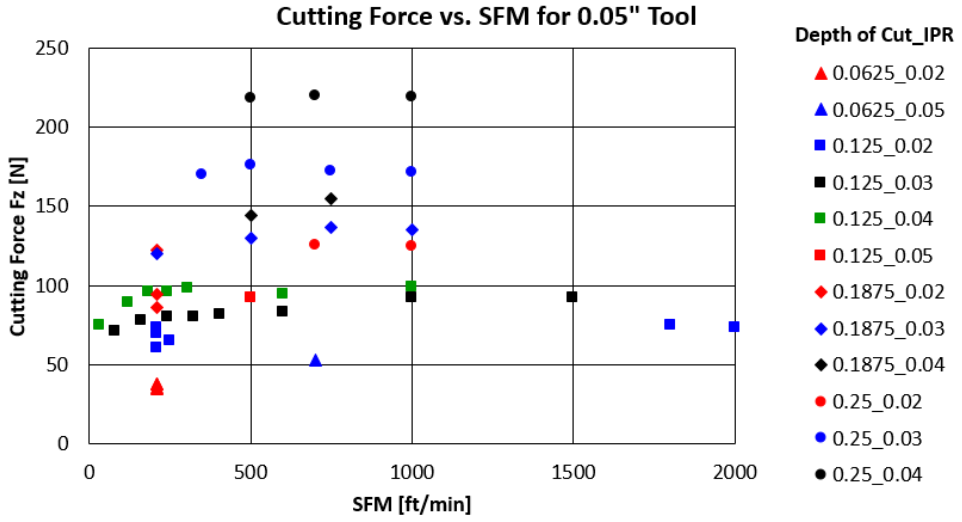

Figure 4.10. Cutting Force Vs. SFM for 0.05" Tool

Figure 4.10 shows the force trends for the 0.005-inch radius tool as SFM is increased while keeping DoC and IPR constant. Shapes denote the DoC while colors denote the IPR.

Figure 4.9 and 4.10 show the same points recorded for all 8 billets of PBX 9501 as in Figures 4.5 and 4.6, however the trends are now plotted against the cutting force instead of the temperature. Like the previous figures SFM is increased along the x-axis while DoC and IPR are kept constant in each trend. It can be observed from these graphs that though the cutting force changes slightly as SFM increases, it generally does not influence how much force is acting on the cutting tool. Thus, the power exerted on the machining increases pretty much linearly with the SFM as one would expect (power = force times velocity). Changing DoC and IPR however, do tend to show an increase in cutting force as they are increased between trends.

The following figure shows a force comparison between the two different radii tools used during the experiment with the same DoC and IPR.

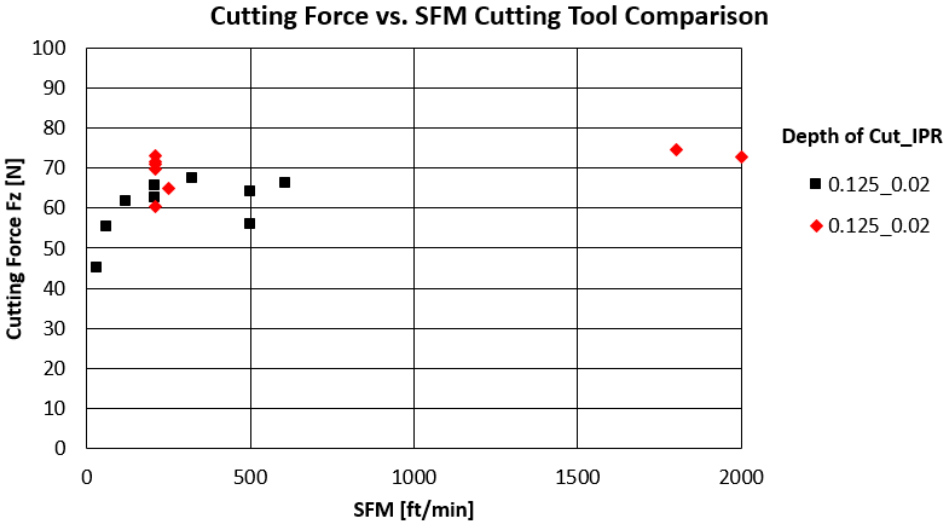

Figure 4.11. Cutting Force Vs. SFM Cutting Tool Comparison. The 0.05-inch radius tool is represented by squares while the 0.005-inch radius tool is represented by diamonds.

Figure 4.11 shows the force comparison between the 0.005-inch radius tool and the 0.05-inch radius tool. The two plots have the same DoC and IPR with a varying SFM. The comparison shows that the force exerted on the cutting tool is approximately the same between the two tools leading to a small variation in force due to tool shape.

4.3 Effects of Machining Parameters

Investigating how the machining parameters DoC, SFM, and IPR affected the temperature and forces of the machining process was the primary scope of this experiment. The combination of these three parameters give a resultant MRR as described in section 2.2.2. the following figures show temperature and cutting force plotted against MRR.

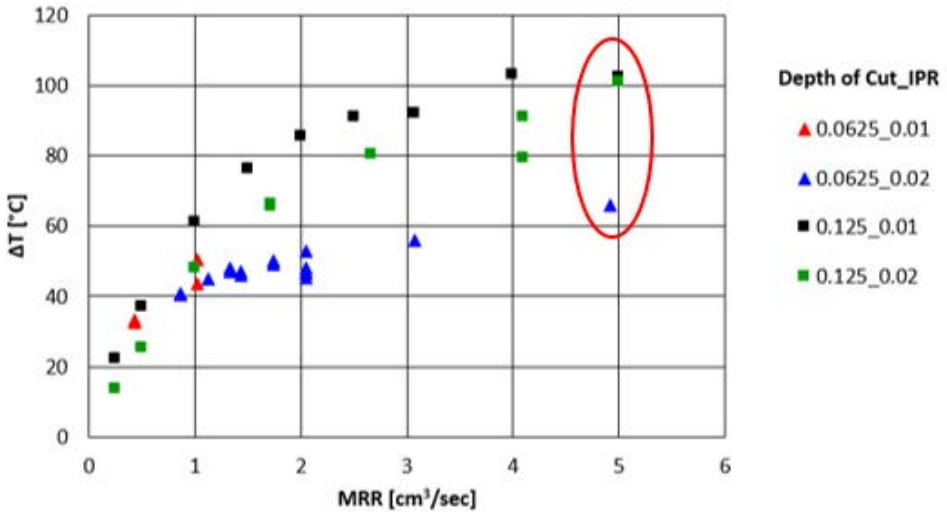

Figure 4.12. Temperature Vs. MRR for 0.005" Tool

Figure 4.12 shows the temperature trends for the 0.005-inch radius tool as MRR is increased while keeping DoC and IPR constant. Shapes denote the DoC while colors denote the IPR. The data points circled in the figure will be used for comparison in Table 4.1.

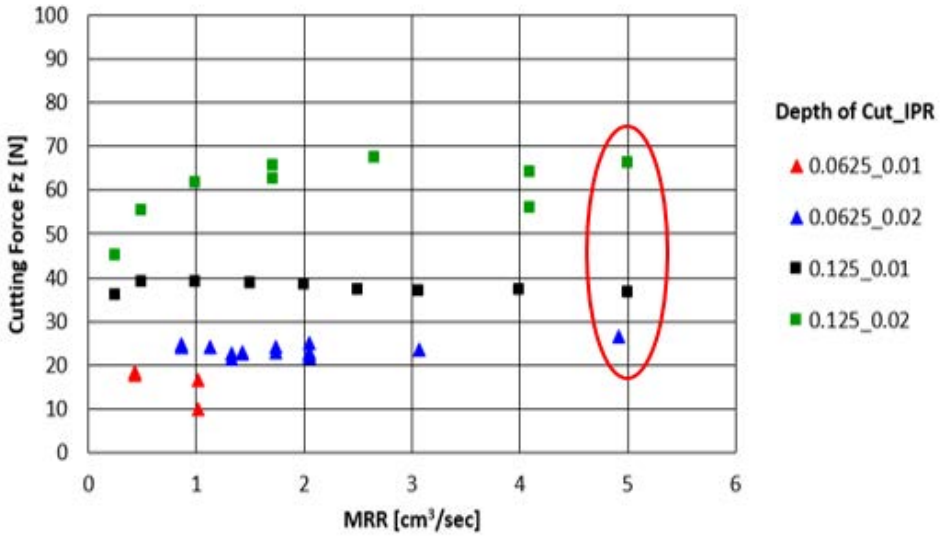

Figure 4.13. Cutting Force Vs. MRR for 0.005" Tool

Figure 4.13 shows the cutting force trends for the 0.005-inch radius tool as MRR is increased while keeping DoC and IPR constant. Shapes denote the DoC while colors denote the IPR. The data points circled in the figure will be used for comparison in Table 4.1.

The above figures show how two trends can have the same MRR, but have very different temperature and forces associated with them. Achieving the same MRR for different DoC and IPR parameters is done by increasing or decreasing the SFM maintained throughout the cut. It can be observed from these figures that shallow depths of cut combined with lower inches per revolution are ideal for keeping temperature and cutting force low during the machining process. An example of some data points with approximately the same MRR are compared in Table 4.1 below.

Table 4.1. Effect of MRR on Temperature and Cutting Force

Parameters	Triangle	Dark Square	Light Square
$MRR\ (cm^3/sec)$	4.9	5	5
$MRR\ (in^3/sec)$	0.299	0.305	0.305
$DoC\ (in)$	0.0625	0.125	0.125
$IPR\ (in)$	0.02	0.01	0.02
$SFM\ (ft/min)$	1200	1220	610
$RPM\ (rev/min)$	1612	1124	639
$Change\ in\ Temperature\ (K)$	66	102	101
$Cutting\ Force\ (N)$	27	36	66
$Measured\ Power\ (W)$	160	225	200

From the above table, it is observed that though the amount of material being removed is approximately the same for all three columns, it is easier on the cutting tool to machine with the initial parameters given in the first column. There is also less power associated with the first column of data resulting in the lower heat and force components.

An additional component that was measured was the torque applied to the cutting tool during machining. The dynamometer measured the torques in the x-, y-, and z-directions and this data was recoreded as well. The following figure shows some force measurements that were taken during the machining process.

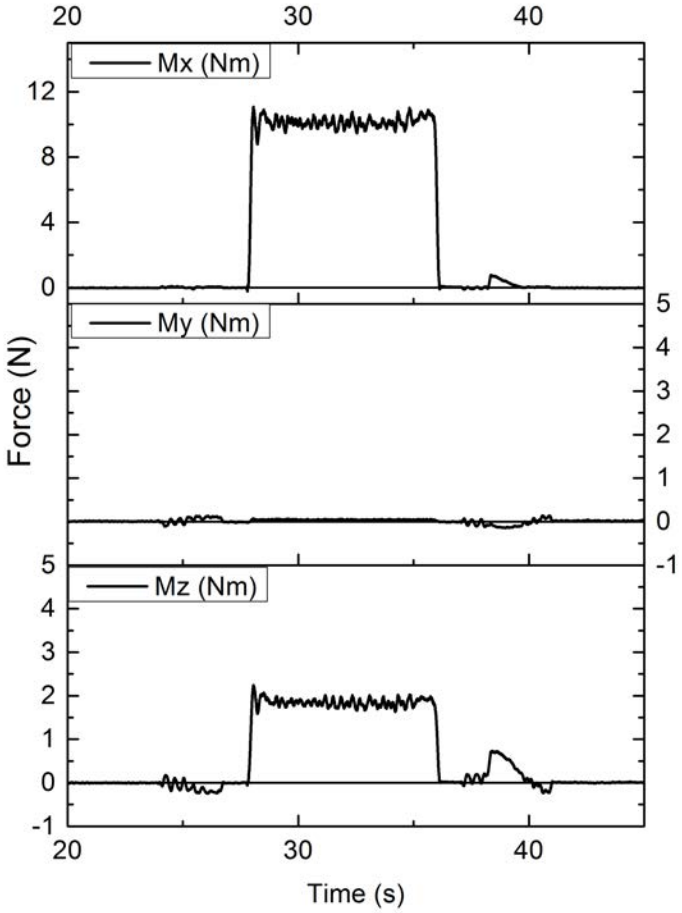

Figure 4.14. Billet 3 Trial 12 Torque Measurements for 0.005" Tool

Figure 4.14 shows the torque measurements taken using the dynamometer during a machining pass. The initial machining parameters were a 500 SFM, 0.02 IPR, and a 0.125 DoC. Majority of the torque acting on the cutting tool is applied around the x-axis. A typical value measured for the torques on the cutting tool for this experiment were 10 $N \cdot m$ in the x-component and 2 $N \cdot m$ in the z-component.

In addition to the measurement of the torque applied to the tool, the torque applied to the workpiece was also calculated using the following equation.

$$Torque = F_c \cdot \frac{radius_{initial} + radius_{cut}}{2} \tag{4.2}$$

Equation 4.2 above was used to approximate the amount of torque applied to the workpiece during machining in the x-component. This equation takes the maximum cutting force measured on the cutting tool, then multiplies this force to the average of the sum of the radius of the workpiece before and after a pass. A typical range of calculated torque values on the workpiece for this experiment were 1 to 3 $N \cdot m$, with a maximum calculated torque of 10.57 $N \cdot m$. The initial cutting parameters for the maximum calculated torque were a SFM of 1000 $\frac{ft}{min}$, an IPR of 0.04 $\frac{in}{rev}$, and a DoC of 0.25 inches off of the diameter of the workpiece. The results of this experiment indicated a larger cutting depth would result in a higher amount of torque applied to both the tool and the workpiece.

Horse power was one of the quantities that was taken into consideration at the beginning of the project. From past experimental force data, the maximum horse power to conduct this experiment was calculated to be 2.555 HP as described in section 3.1.1. The maximum calculated horse power that used in this experiment was 1.492 HP. The highest measured force and SFM associated with this HP was 218.97 N and 1000 $\frac{ft}{min}$.

CHAPTER 5
Conclusion

The machining parameters DoC, IPR, and SFM define the temperature and force components exerted on the cutting tool during the machining of PBX 9501. The temperature component at the cutting interface during the machining process is most sensitive to changes in DoC and SFM, while insensitive to changes in IPR. The cutting force component is more sensitive to changes DoC and IPR, while less sensitive to changes in SFM. To reduce the amount of time it takes to machine a billet of PBX 9501, while also keeping the force and temperatures low during the process, a shallow DoC, low IPR, and high SFM are desirable. This will provide a high MRR which will reduce the time taken to machine a billet of PBX, while also staying within a safe boundary for the force and temperature components.

5.1 Future Work

Future work for this experiment will include initial characterization of PBX 9502 to be performed in the near future. Data will be recorded using the same process as described in this thesis by studying the effects of DoC, IPR, and SFM on the temperature and forces acting on the cutting tool during the machining process. Other work could be to machine high explosives other than PBX to gain insight into the characterization of different types of high explosives.

BIBLIOGRAPHY

[1] *DOE-STD-1212-2012*, 2012.

[2] Mikell P. Groover. *Fundamentals of Modern Maunufacturing, 4th Edition*. John Wiley & Sons, 2010.

[3] Süleyman Yaldız and Faruk Ünsaçar. Design, development and testing of a turning dynamometer for cutting force measurement. *Materials & design*, 27(10):839–846, 2006.

[4] Paul A Urtiew, Kevin S Vandersall, Craig M Tarver, and Frank Garcia. Initiation of heated pbx-9501 explosive when exposed to dynamic loading. In *Report: UCRL-CONF-214667, Lawrence Livermore National Laboratory*, 2005.

[5] Jack R. Anthony and Robert W. Ashcraft. High explosive machine tool force test. Technical report, Mason & Hanger - Silas Mason Co. Inc., September 1988.

[6] *DOE M 440. 1-1*, September 1995.

[7] Brigitta M Dobratz. Properties of chemical explosives and explosive simulants. Technical report, comp. and ed.; California Univ., Livermore (USA). Lawrence Livermore Lab., 1972.

[8] PJ Rae, SJP Palmer, HT Goldrein, JE Field, and AL Lewis. Quasi–static studies of the deformation and failure of pbx 9501. In *Proceedings of the Royal Society of London A: Mathematical, Physical and Engineering Sciences*, volume 458, pages 2227–2242. The Royal Society, 2002.

[9] Zhao Xiao-dong. Experimental and numerical investigation into machining parameters for cutting forcers and temperatures of pbx [a]. wang ya-jun, huang ping, li sheng-cai. theory and practice of energetic materials [c], 2005.

[10] Baileigh Industrial. *Metal Lathe Model: PL-1640 Operator's Manual*, 10-2013 edition, 2013.

[11] *DURApulse AC Drives User Manual*, 1st ed. rev. d edition, May 2013.

[12] MA Davies, T Ueda, R M'saoubi, B Mullany, and AL Cooke. On the measurement of temperature in material removal processes. *CIRP Annals-Manufacturing Technology*, 56(2):581–604, 2007.

AppendixA

Tool Radius [in]	RPM [rev/min]	SFM [ft/min]	IPR [in]	DoC [in]	Fx [N]	Fy [N]	Fz [N]	Torque [N*m]	ΔT1 [K]	ΔT2 [K]	Power [W]
0.05	205.78	210.00	0.02	0.0625	0.00	-13.98	34.60	1.69	40.45	17.99	36.91
0.05	212.60	210.00	0.02	0.0625	-0.47	-15.36	37.80	1.78	40.46	18.76	40.33
0.05	219.88	210.00	0.02	0.0625	0.00	-14.21	35.10	1.60	40.72	19.28	37.44
0.05	227.67	210.00	0.02	0.0625	0.00	-14.80	37.91	1.67	66.24	33.85	40.44
0.05	236.04	210.00	0.02	0.1250	-8.86	-22.70	71.00	2.95	65.58	33.21	75.74
0.05	254.78	210.00	0.02	0.1250	-8.52	-22.00	69.65	2.68	80.61	49.16	74.30
0.05	276.74	210.00	0.02	0.1250	-8.03	-21.00	71.67	2.53	79.35	48.77	76.46
0.05	302.85	210.00	0.02	0.1250	-9.15	-20.50	72.99	2.34	80.07	48.80	77.87
0.05	334.39	210.00	0.02	0.1250	-8.72	-17.87	60.56	1.75	33.25	15.03	64.61
0.05	373.28	210.00	0.02	0.1875	-21.47	-28.85	122.00	3.04	32.65	15.14	130.15
0.05	452.14	210.00	0.02	0.1875	-19.74	-29.29	94.60	1.91	46.09	18.35	100.92
0.05	573.25	210.00	0.02	0.1875	-21.63	-27.14	85.70	1.32	46.98	18.86	91.42
0.005	198.90	210.00	0.02	0.0625	-2.71	-5.73	24.74	1.25	40.45	17.99	26.39
0.005	205.26	210.00	0.02	0.0625	-2.61	-5.59	24.06	1.18	40.46	18.76	25.67
0.005	212.03	210.00	0.02	0.0625	-2.61	-5.44	24.06	1.14	40.72	19.28	25.67
0.005	219.28	210.00	0.02	0.1250	-12.70	-11.30	65.70	2.95	66.24	33.85	70.09
0.005	235.35	210.00	0.02	0.1250	-11.96	-11.16	62.40	2.60	65.58	33.21	66.57
0.005	253.97	210.00	0.02	0.1875	-22.45	-14.77	100.35	3.79	80.61	49.16	107.05
0.005	288.17	210.00	0.02	0.1875	-22.23	-16.02	104.64	3.45	79.35	48.77	111.63
0.005	333.01	210.00	0.02	0.1875	-23.48	-15.09	102.06	2.88	80.07	48.80	108.88
0.005	414.97	210.00	0.01	0.0625	-3.70	-4.60	18.51	0.44	33.25	15.03	19.75
0.005	443.64	210.00	0.01	0.0625	-3.48	-4.45	17.76	0.39	32.65	15.14	18.95
0.005	794.29	350.00	0.02	0.0625	-2.16	-4.52	22.67	0.47	46.09	18.35	40.31
0.005	857.97	350.00	0.02	0.0625	-2.32	-4.44	22.91	0.44	46.98	18.86	40.73
0.005	1332.52	500.00	0.01	0.0625	-3.38	-3.73	19.04	0.33	50.32	20.18	48.36

Figure 5.1. HE Machining Results Spreadsheeet 1 of 4

0.005	1459.76	500.00	0.02	0.0625	-2.06	-4.76	23.03	0.36	46.85	16.86	58.50
0.005	1613.88	500.00	0.02	0.0625	-2.21	4.40	21.75	0.31	47.98	17.81	55.25
0.005	1804.37	500.00	0.02	0.0625	-2.00	-4.56	22.76	0.29	46.52	16.42	57.81
0.005	2045.85	500.00	0.02	0.0625	-1.87	-4.20	21.90	0.24	45.32	16.56	55.63
0.005	2338.83	500.00	0.02	0.0625	-1.96	-4.58	22.45	0.22	39.31	9.61	57.02
0.005	249.63	275.00	0.02	0.0625	-2.62	-5.17	24.21	1.28	44.66	19.62	33.82
0.005	304.05	325.00	0.02	0.1250	-12.54	-10.47	67.46	3.39	80.44	43.96	111.38
0.005	323.19	325.00	0.02	0.0625	-2.13	-4.72	21.45	1.03	45.57	19.7	35.41
0.005	334.06	325.00	0.02	0.0625	-2.66	-4.96	22.56	1.05	48.84	21.68	37.25
0.005	452.05	425.00	0.02	0.0625	-2.70	-5.20	24.16	1.08	50.51	21.22	52.16
0.005	468.34	425.00	0.02	0.0625	-2.70	-5.10	22.91	0.99	50.38	21.97	49.46
0.005	571.59	500.00	0.02	0.0625	-2.56	-5.20	24.92	1.04	52.21	21.48	63.30
0.005	593.42	500.00	0.02	0.1250	-11.42	-9.27	63.99	2.52	90.69	48.76	162.53
0.005	965.06	750.00	0.02	0.0625	-2.39	-5.67	23.56	0.87	55.91	21.62	89.76
0.005	1611.95	1200.00	0.02	0.0625	-3.34	-4.76	26.44	0.93	66.85	24.23	161.18
0.005	1053.77	750.00	0.01	0.1250	-8.64	-5.29	36.69	1.21	92.14	49.85	139.79
0.005	773.61	500.00	0.02	0.2500	-24.8	-12.83	121.97	3.44	106.34	77.7	309.80
0.005	969.96	500.00	0.02	0.2500	-24.48	-12.92	119.52	2.61	103.55	74.04	303.58
0.005	1299.88	500.00	0.02	0.1250	-10.21	-9	55.77	0.95	79.47	36.54	141.66
0.005	1566.25	500.00	0.01	0.0625	-3.23	-3.85	16.44	0.24	43.47	17.13	41.76
0.005	1745.05	500.00	0.02	0.0625	-2.2	-4.6	21.33	0.28	42.17	15.37	54.18
0.005	1969.93	500.00	0.02	0.0625	-2.3	-4.76	22.83	0.26	25.44	4.83	57.99
0.005	1123.47	1220.00	0.01	0.1250	-9.59	-5.92	36.45	1.86	102.43	55.31	225.90
0.005	956.39	976.00	0.01	0.1250	-10.24	-5.92	37.16	1.78	103.11	56.707	184.24
0.005	638.69	610.00	0.02	0.1250	-11.5	-9.77	66.08	2.96	101.06	54.39	204.77
0.005	685.65	610.00	0.01	0.1250	-9.45	-6.24	37.04	1.54	91.14	49.85	114.78
0.005	592.05	488.00	0.01	0.1250	-9.83	-6.57	38.40	1.48	85.36	47.06	95.20
0.005	482.32	366.00	0.01	0.1250	-10.49	-6.93	38.75	1.37	76.32	40.92	72.05
0.005	351.88	244.00	0.01	0.1250	-11.17	-7.21	39.10	1.25	61.05	32.12	48.47

Figure 5.2. HE Machining Results Spreadsheeet 2 of 4

0.005	194.27	122.00	0.02	0.1250	-12.99	-13.87	61.51	1.78	48.21	24.09	38.12
0.005	216.86	122.00	0.01	0.1250	-11.72	-9.12	39.10	1.01	36.91	19.77	24.23
0.005	122.70	61.00	0.02	0.1250	-11.04	-14.67	55.23	1.25	25.23	12.5	17.11
0.005	141.29	61.00	0.01	0.1250	-11.71	-9.72	35.94	0.70	22.37	12.04	11.14
0.005	81.89	30.00	0.02	0.1250	-9.09	-14.56	44.86	0.73	13.72	6.8	6.84
0.05	276.87	305.00	0.04	0.1250	-7.05	-24.09	98.26	5.10	92.67	59.8	152.24
0.05	392.78	407.00	0.03	0.1250	-7.7	-20.6	81.72	3.98	88.9	59.56	168.96
0.05	251.34	244.00	0.04	0.1250	-5.91	-25.32	95.93	4.37	89.37	56.74	118.91
0.05	360.08	326.00	0.03	0.1250	-7.18	-21.04	79.61	3.37	88.22	56.50	131.84
0.05	250.01	210.00	0.02	0.1250	-8.96	-20.39	64.82	2.54	65.53	40.81	69.15
0.05	236.27	183.00	0.04	0.1250	-6.86	-28.48	95.50	3.44	79.97	45.93	88.78
0.05	344.09	244.00	0.03	0.1250	-7.77	-22.86	79.78	2.62	84.47	45.53	98.89
0.05	189.53	122.00	0.04	0.1250	-6.50	-30.81	89.38	2.65	66.47	34.58	55.39
0.05	281.87	163.00	0.03	0.1250	-7.47	-26.02	77.92	2.06	72.50	34.28	64.52
0.05	118.94	61.00	0.04	0.1250	N/A	N/A	N/A	N/A	45.16	21.56	N/A
0.05	181.03	81.00	0.03	0.1250	-8.07	-28.08	71.25	1.43	45.52	20.98	29.32
0.05	81.14	31.00	0.04	0.1250	-5.98	-32.51	74.68	1.27	23.74	8.95	11.76
0.05	923.11	1000.00	0.04	0.1250	-7.05	-96.69	99.07	5.05	94.84	46.84	503.28
0.05	982.43	1000.00	0.03	0.1250	-8.65	-92.1	91.77	4.39	94.62	52.23	466.19
0.05	629.94	600.00	0.04	0.1250	-6.63	-23.28	94.21	4.21	90.76	51.35	287.15
0.05	676.40	600.00	0.03	0.1250	-8.45	-21.88	83.21	3.45	89.92	54.52	253.62
0.05	1217.09	1000.00	0.03	0.1875	-18.39	-35.94	135.24	5.07	110.52	73.14	687.02
0.05	1036.62	750.00	0.03	0.1875	-20.42	-26.09	136.72	4.48	106.75	75.44	520.90
0.05	1199.26	750.00	0.04	0.1875	-19.41	-30.31	154.77	4.33	104.68	90.70	589.67
0.05	948.30	500.00	0.04	0.1875	-18.19	-31.02	144.49	3.35	95.93	81.71	367.00
0.05	1165.14	500.00	0.03	0.1875	-20.02	-26.79	130.21	2.40	94.84	76.13	330.73
0.05	634.43	210.00	0.03	0.1875	-19.81	-31.02	120.08	1.64	83.61	54.04	128.10
0.05	1384.66	1500.00	0.03	0.1250	-9.65	-129.46	92.13	4.70	94.88	46.74	702.03
0.05	1964.86	2000.00	0.02	0.1250	-19.84	-120.33	72.89	3.49	92.91	43.2	740.56

Figure 5.3. HE Machining Results Spreadsheeet 3 of 4

0.05	1768.38	1800.00	0.02	0.1250	-21.64	-122.39	74.69	3.57	95.33	46.5	682.97
0.05	734.93	700.00	0.05	0.0625	-3.15	-16.2	53.01	2.41	87.11	38.99	188.50
0.05	543.62	500.00	0.03	0.2500	-30.69	-31.37	175.77	7.29	111.26	89.35	446.46
0.05	1267.55	1000.00	0.03	0.2500	-29.15	-30.47	171.26	6.01	117.28	83.05	870.00
0.05	1139.66	750.00	0.03	0.2500	-29.92	-30.12	172.04	4.95	112.88	83.06	655.47
0.05	663.81	350.00	0.03	0.2500	-31.21	-31.69	169.84	3.81	96.56	79.78	301.98
0.05	1261.27	500.00	0.05	0.1250	-3.89	-23.34	92.19	1.63	77.97	52.14	234.16
0.05	943.62	1000.00	0.04	0.2500	-33.23	-38.86	218.97	10.57	122.47	101.12	1112.37
0.05	753.57	700.00	0.04	0.2500	-32.46	-35.51	219.76	9.21	117.41	107.01	781.47
0.05	626.50	500.00	0.04	0.2500	-31.95	-35.56	218.29	7.76	111.82	108.99	554.46
0.05	1498.69	1000.00	0.02	0.2500	-34.78	-32.11	124.55	3.64	112.08	81.07	632.71
0.05	1304.96	700.00	0.02	0.2500	-29.81	-26.15	125.59	2.87	106.23	78.76	446.60

Figure 5.4. HE Machining Results Spreadsheeet 4 of 4

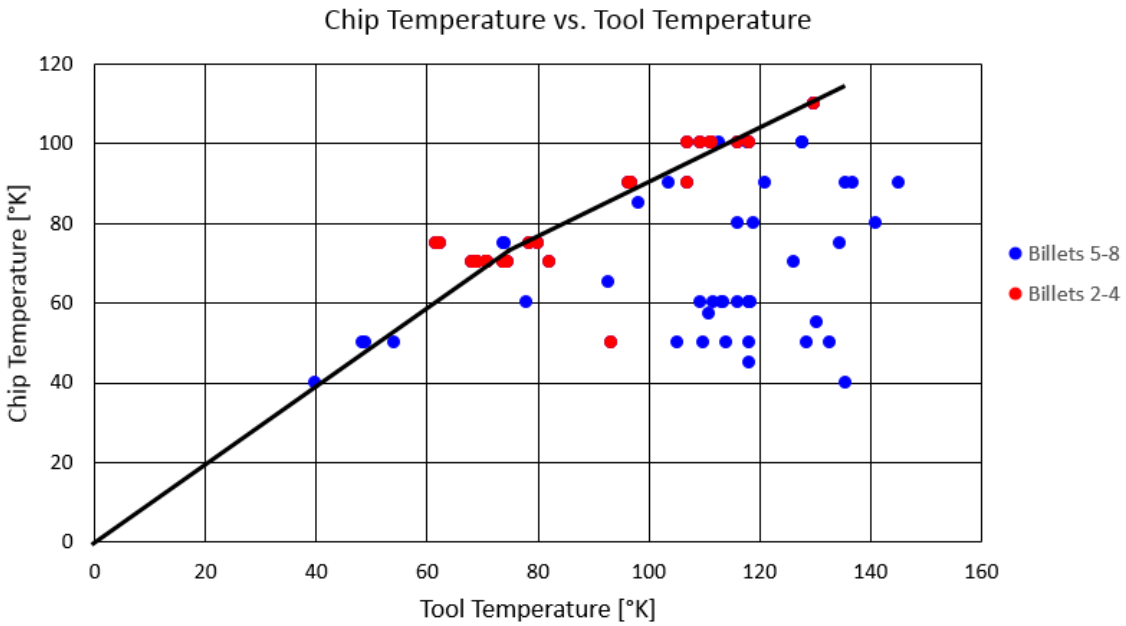

Figure 5.5. Chip Temperature vs. Tool Temperature Comparison for PBX 9501

The above graph shows an approximated temperature trend for the workpiece chip compared to the measured cutting tool temperature. The black line is the best fit approximation for this trend. Billets 5 through 8 were not considered relevant to the trend in this graph due to many outliers and inconclusive IR measurements.

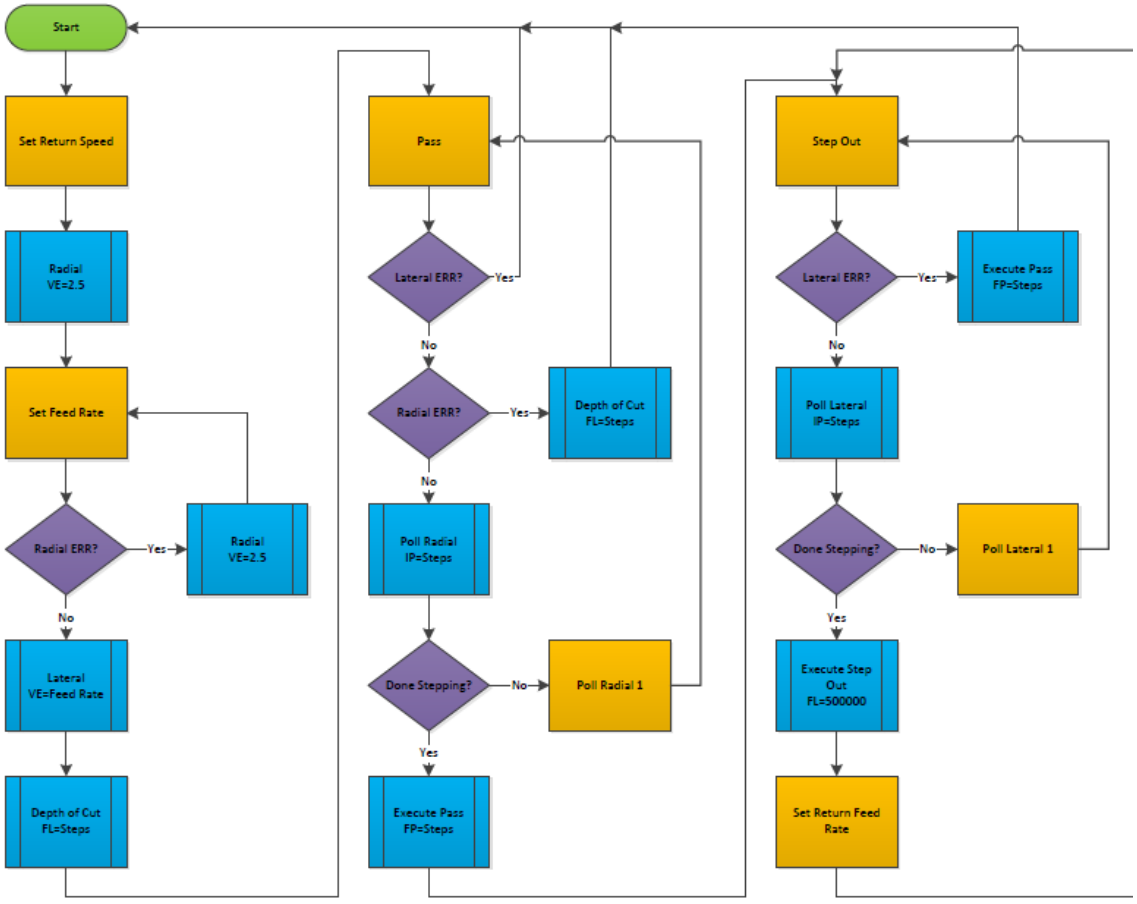

Figure 5.6. Stepper Motor Automated Machining Pass Flowchart Part 1 of 2

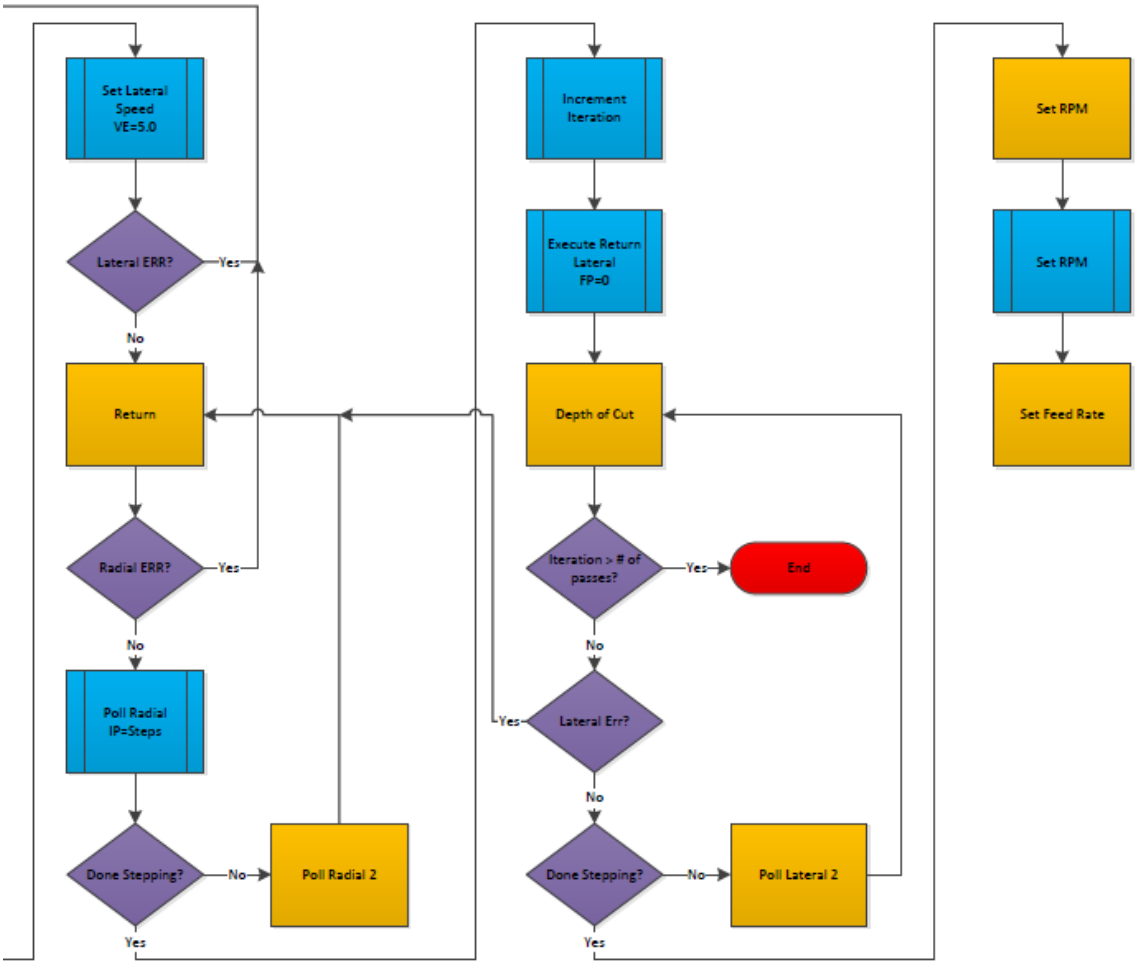

Figure 5.7. Stepper Motor Automated Machining Pass Flowchart Part 2 of 2

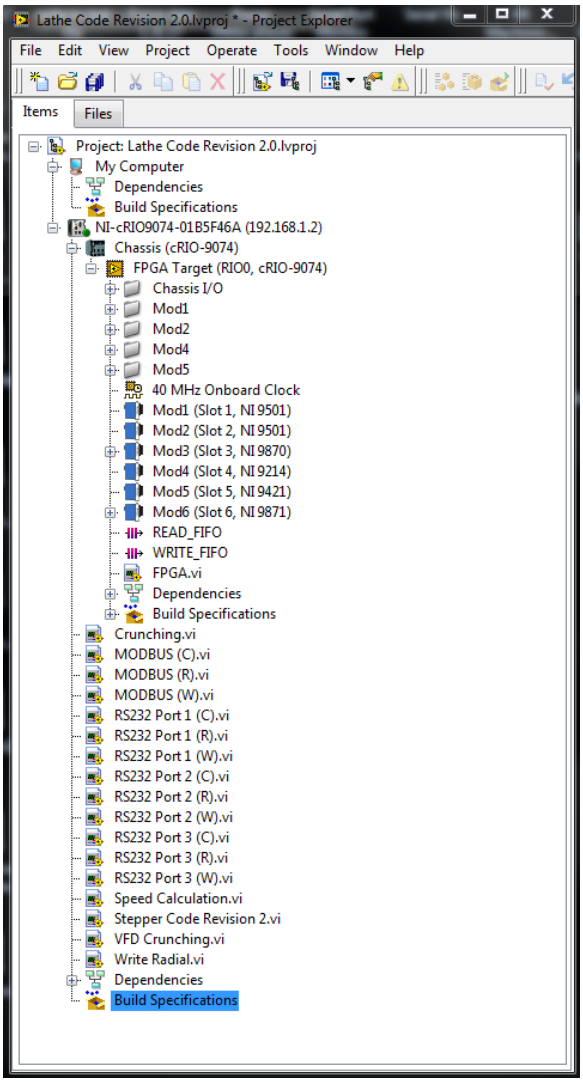

Figure 5.8. LabVIEW Project Tree

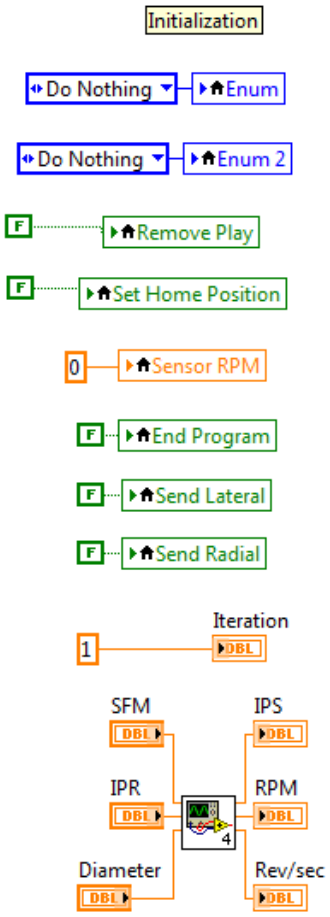

Figure 5.9. LabVIEW Top Code Snippet: Initialization

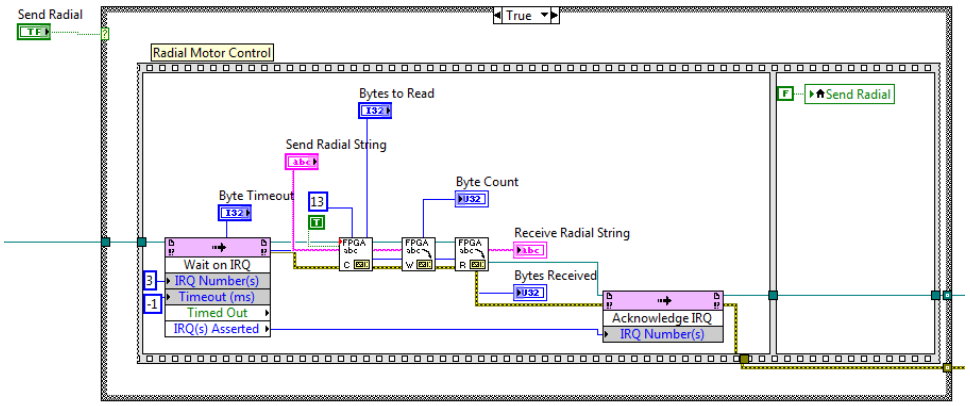

Figure 5.10. LabVIEW Top Code Snippet: Serial Communication

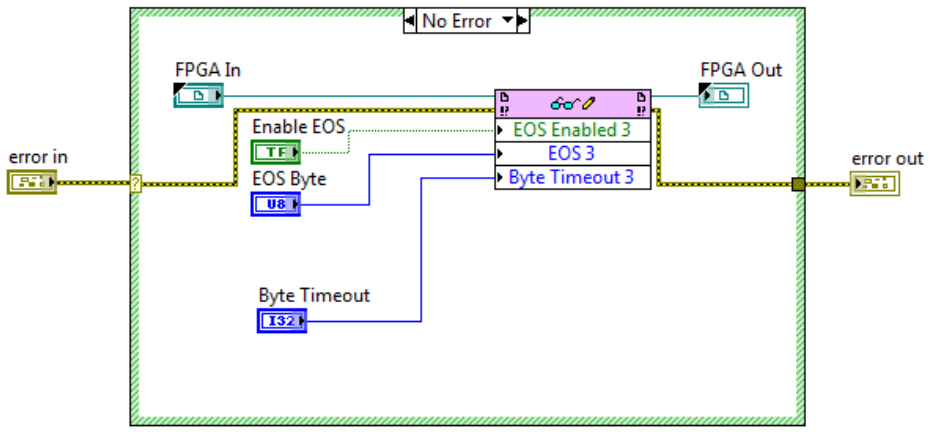

Figure 5.11. LabVIEW Top Code Snippet: Serial Configuration SubVI

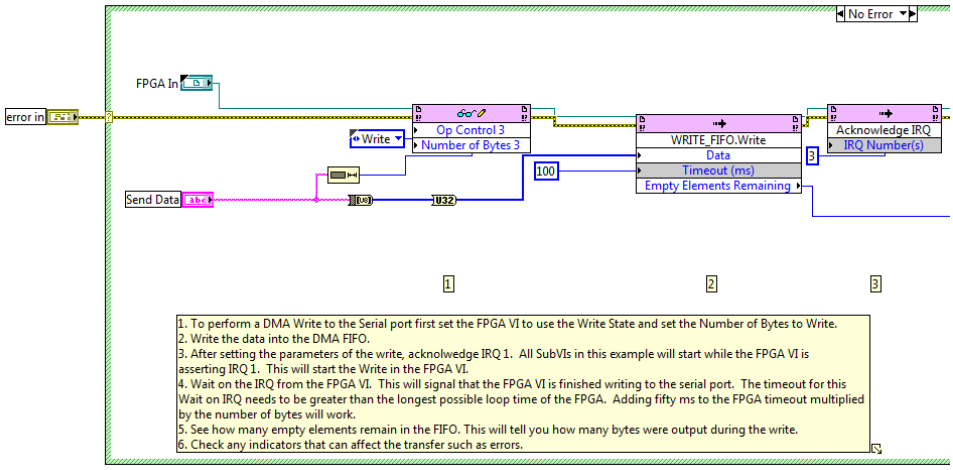

Figure 5.12. LabVIEW Top Code Snippet: Serial Write SubVI Part 1 of 2

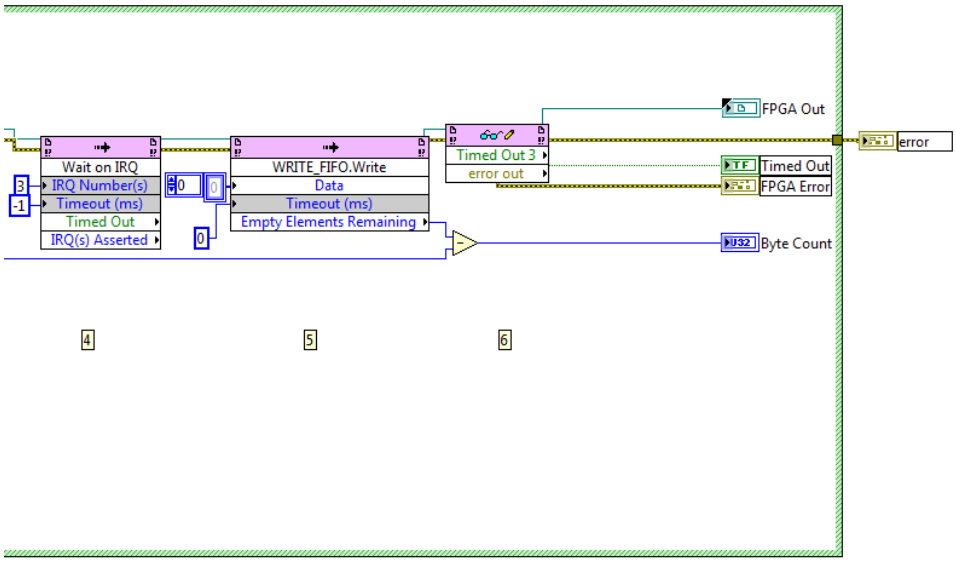

Figure 5.13. LabVIEW Top Code Snippet: Serial Write SubVI Part 2 of 2

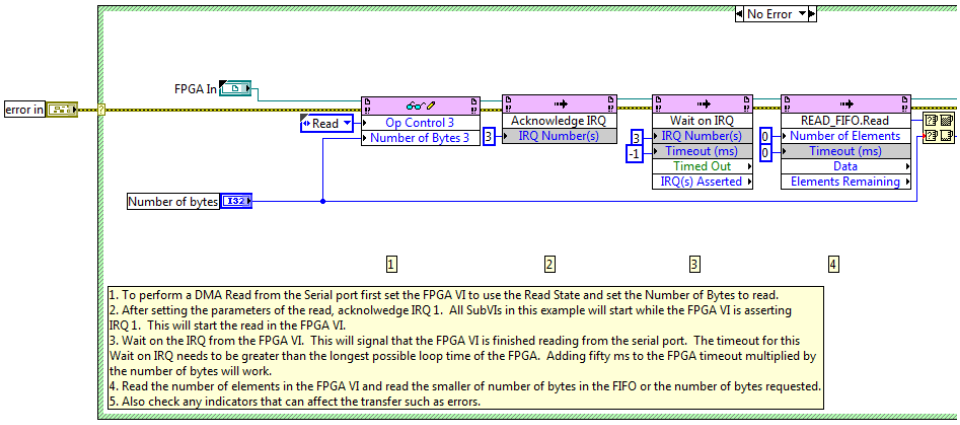

Figure 5.14. LabVIEW Top Code Snippet: Serial Write SubVI Part 1 of 2

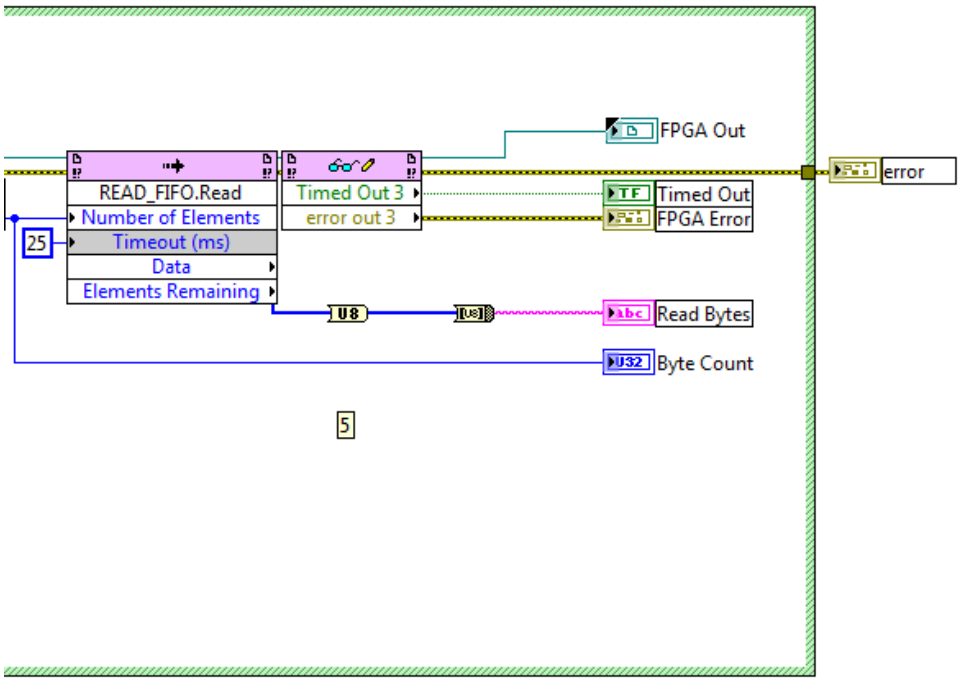

Figure 5.15. LabVIEW Top Code Snippet: Serial Write SubVI Part 2 of 2

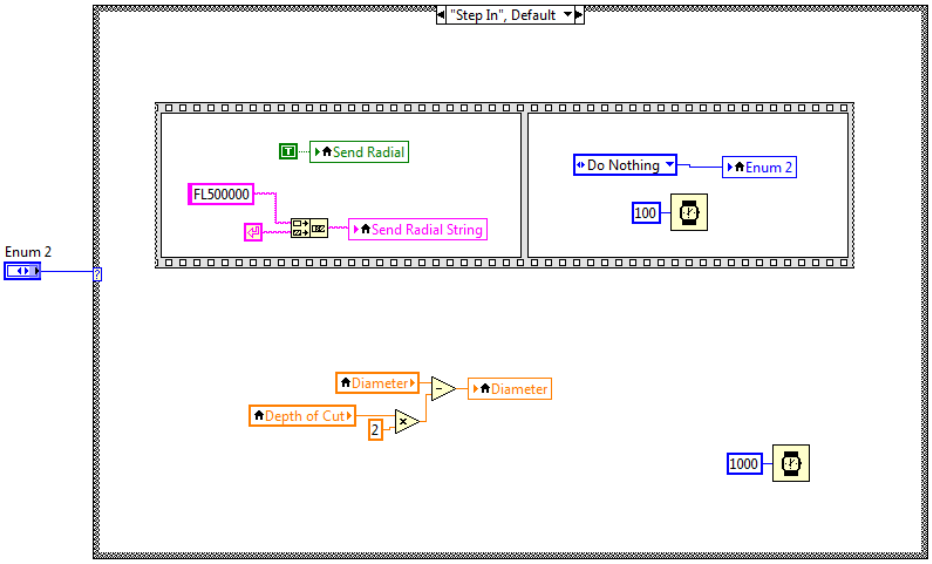

Figure 5.16. LabVIEW Top Code Snippet: Example of One Case for Automated Machining Process

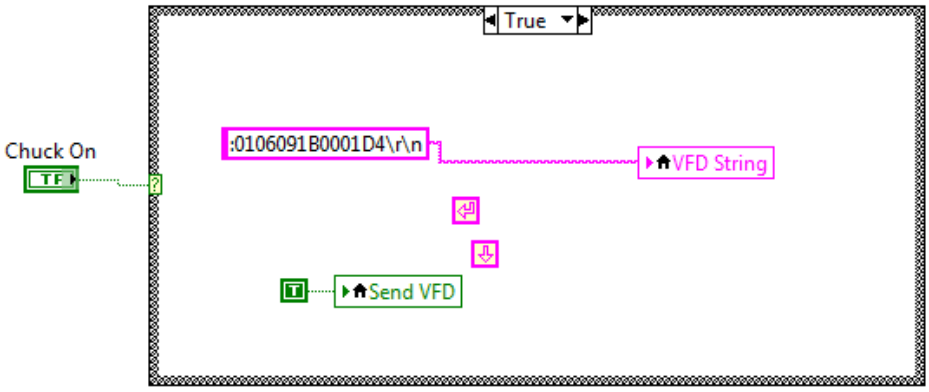

Figure 5.17. LabVIEW Top Code Snippet: Enabling Lathe Chuck Rotation

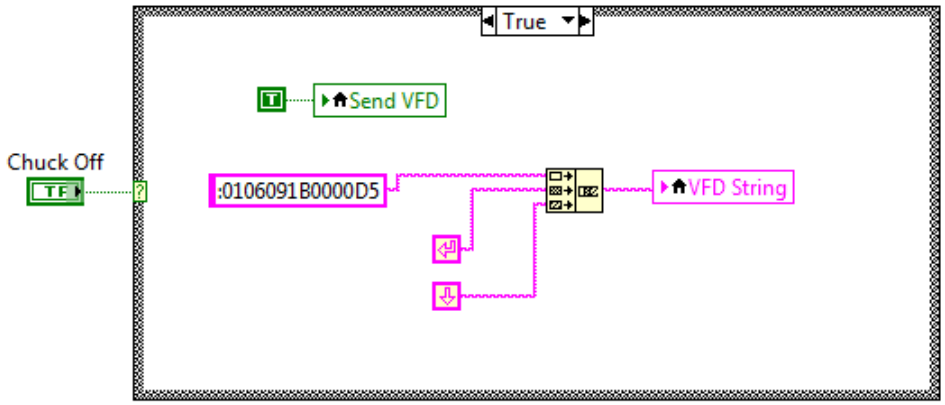

Figure 5.18. LabVIEW Top Code Snippet: Disabling Lathe Chuck Rotation

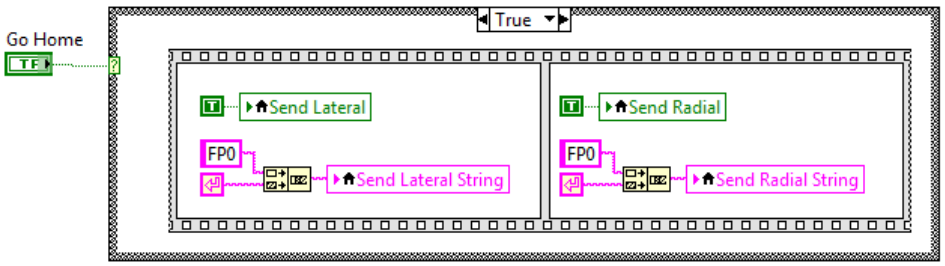

Figure 5.19. LabVIEW Top Code Snippet: Return Saddle to Home Position

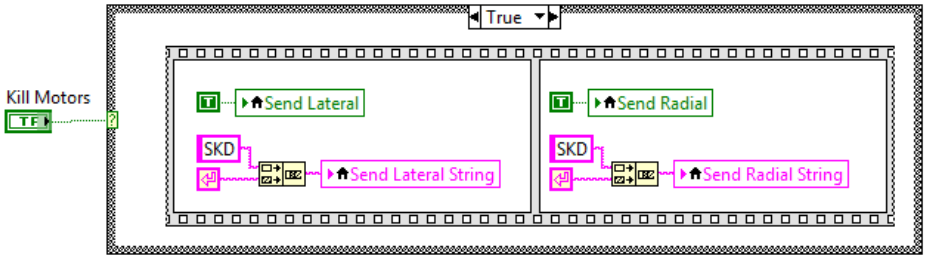

Figure 5.20. LabVIEW Top Code Snippet: Kill Motors and Clear Serial Buffer

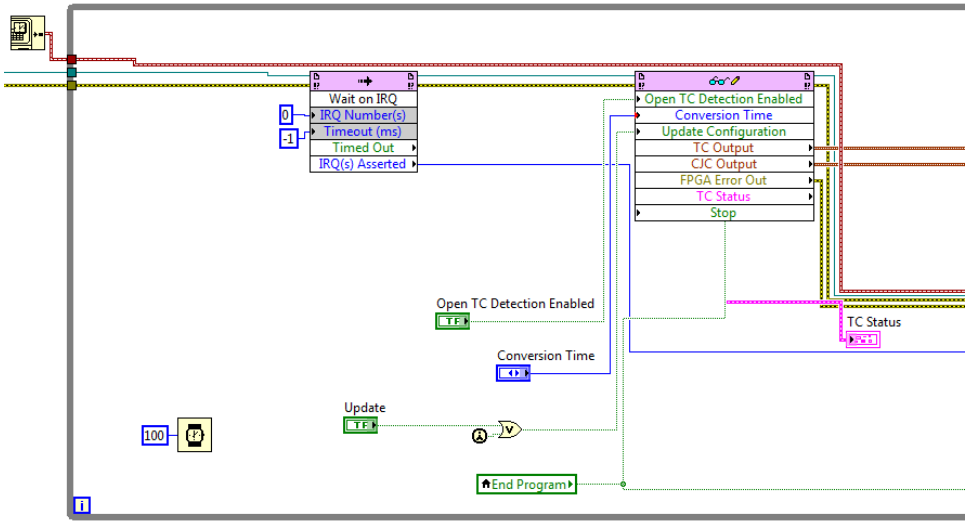

Figure 5.21. LabVIEW Top Code Snippet: Thermocouple Read Function and Graphing Part 1 of 3

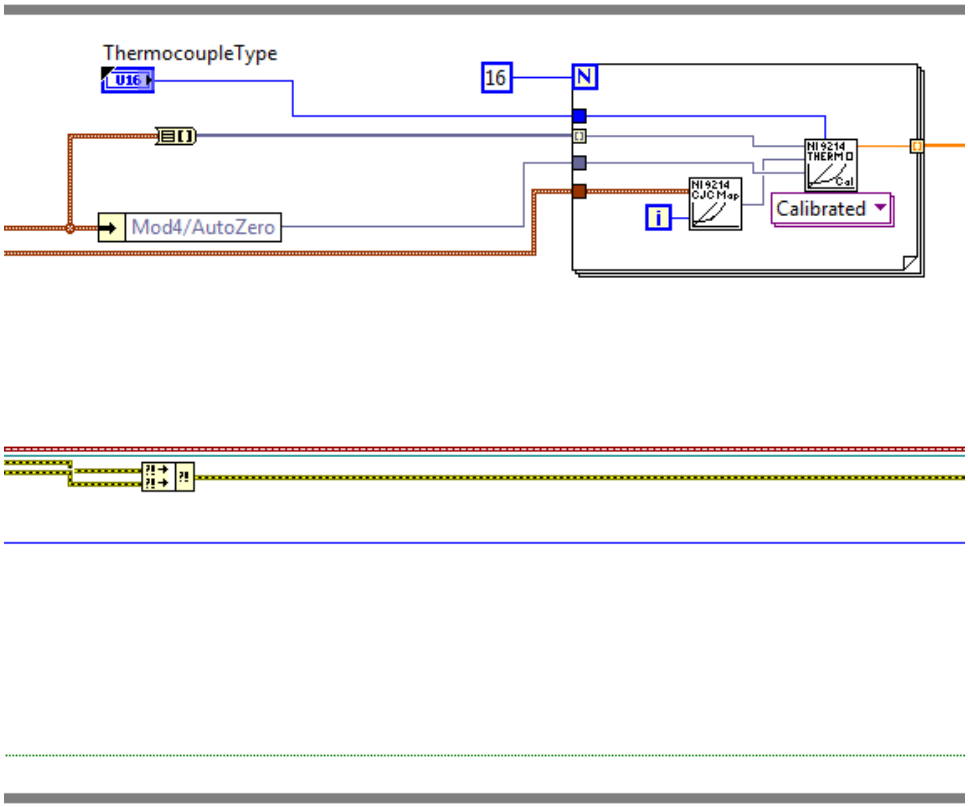

Figure 5.22. LabVIEW Top Code Snippet: Thermocouple Read Function and Graphing Part 2 of 3

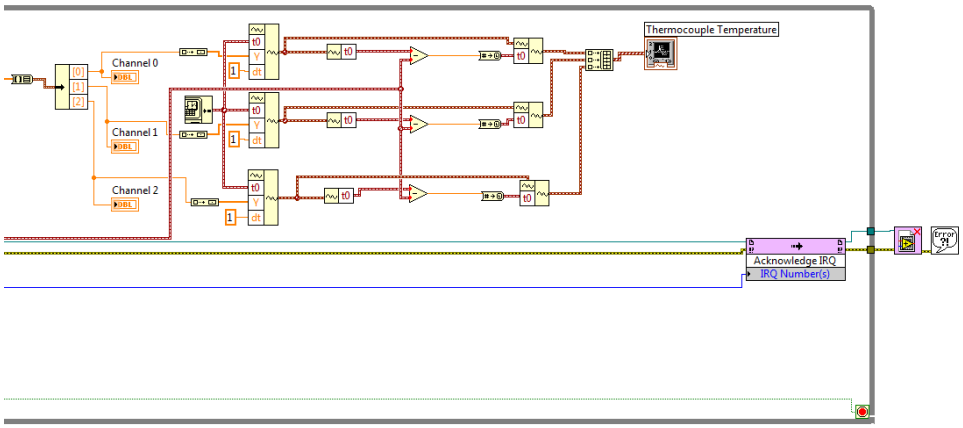

Figure 5.23. LabVIEW Top Code Snippet: Thermocouple Read Function and Graphing Part 3 of 3

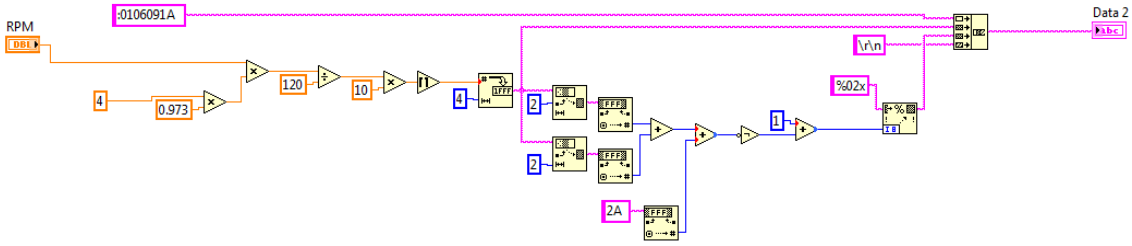

Figure 5.24. LabVIEW Top Code Snippet: Converting LabVIEW Parameters to VDF Serial Commands

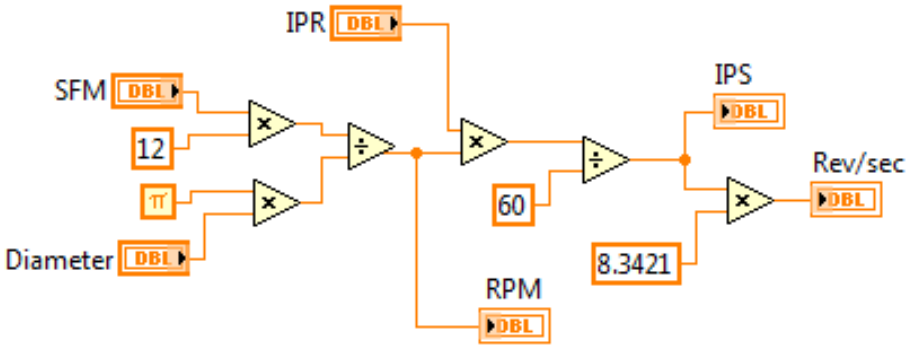

Figure 5.25. LabVIEW Top Code Snippet: Initial Parameter Conversion Calculations

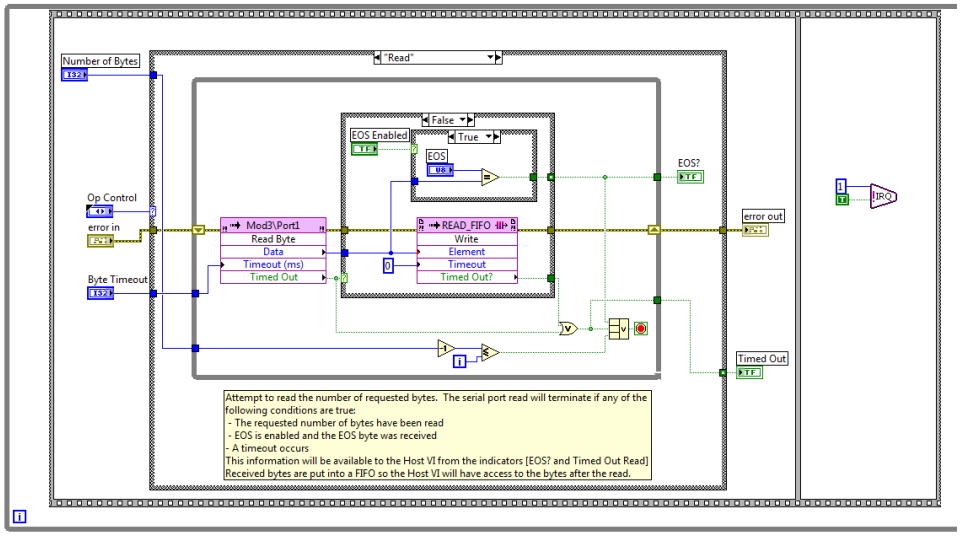

Figure 5.26. LabVIEW FPGA Code Snippet: Serial Port Module Configuration Part 1 of 3

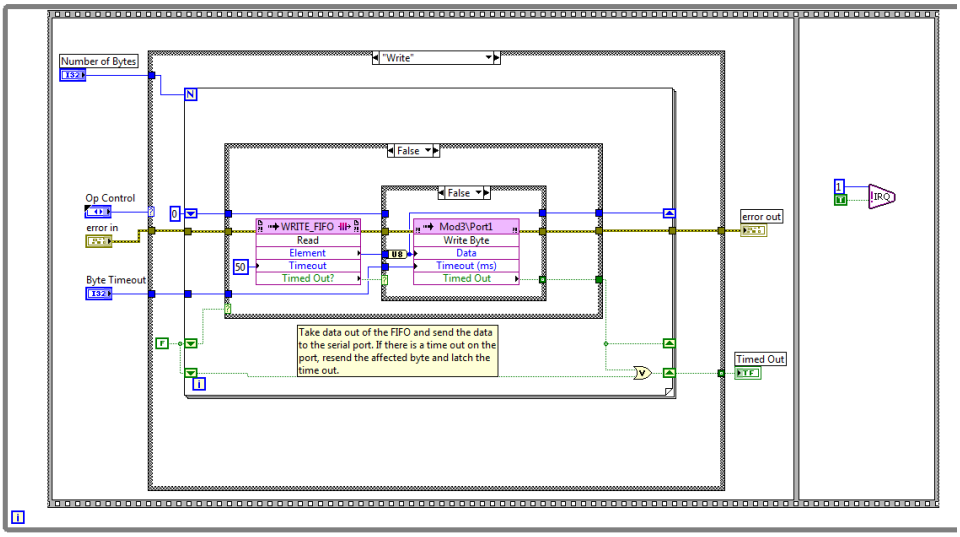

Figure 5.27. LabVIEW FPGA Code Snippet: Serial Port Module Configuration Part 2 of 3

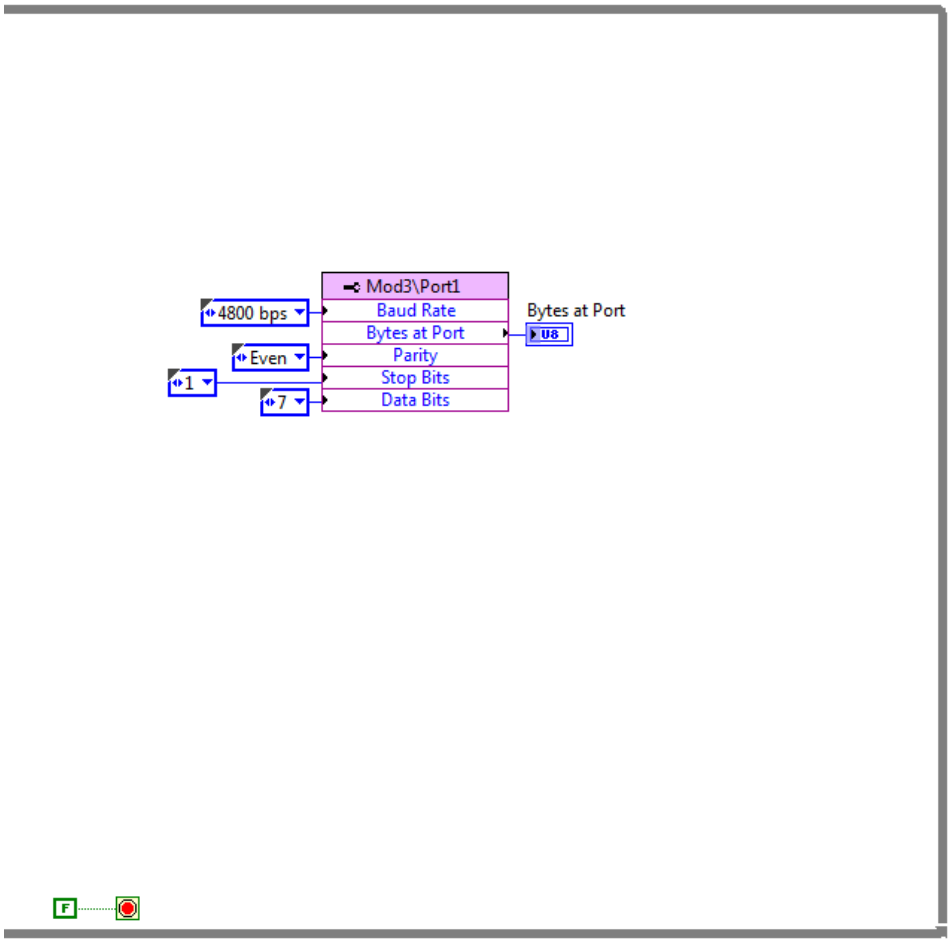

Figure 5.28. LabVIEW FPGA Code Snippet: Serial Port Module Configuration Part 3 of 3

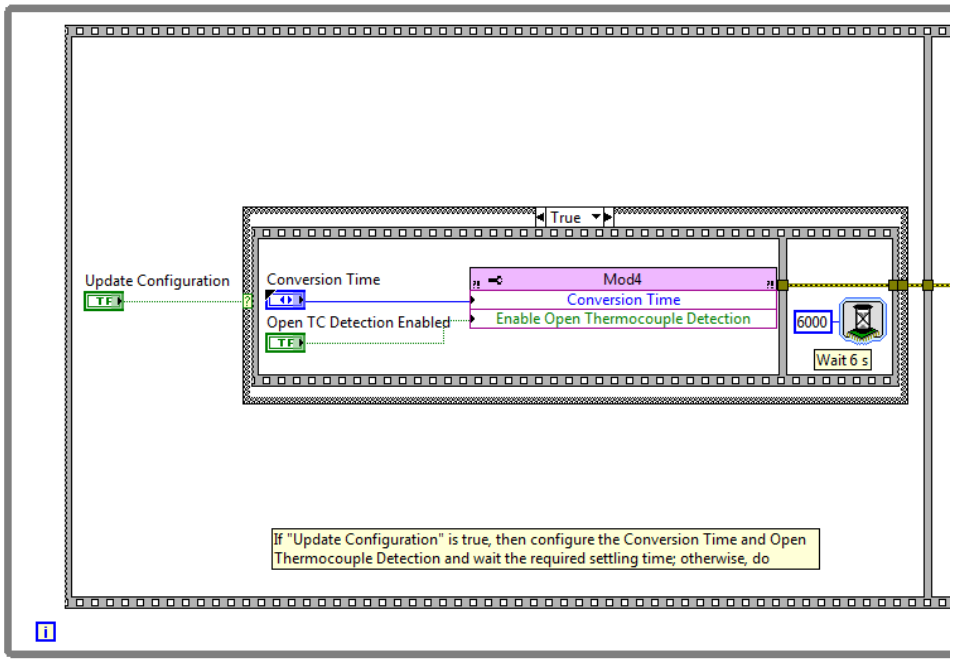

Figure 5.29. LabVIEW FPGA Code Snippet: Thermocouple Module Configuration Part 1 of 2

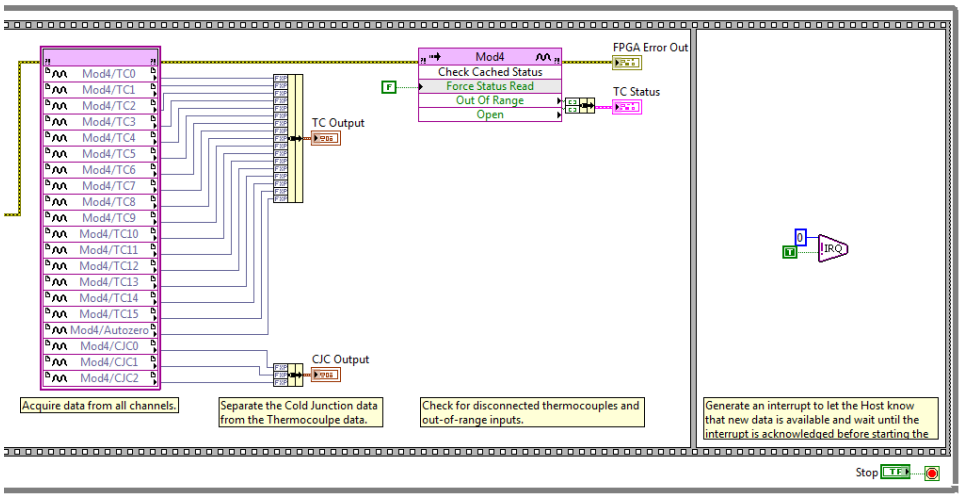

Figure 5.30. LabVIEW FPGA Code Snippet: Thermocouple Module Configuration Part 2 of 2

	A	B	C	D	E	F	G	H	I	J	K	L	M	N
1	Note: Columns 3 to 15 as well as colums 35 and 42 to 43 need to be populated from experiment													
2	Column 42 and 43: from experiment (cols. 40,41) and transient thermal simulation.													
3	Machine Date	4/26/2017	4/26/2017	4/26/2017	4/26/2017	4/26/2017	4/26/2017	4/26/2017	4/26/2017	4/26/2017	4/26/2017	4/26/2017	4/26/2017	4/26/2017
4	Trial	1	2	3	4	5	6	7	8	9	10	11	12	13
5	Pass #	1	1	1	1	1	1	1	1	1	1	1	1	1
6	Material	PBX9501	PBX9501	PBX9501	PBX9501	PBX9501	PBX9501	PBX9501	PBX9501	PBX9501	PBX9501	PBX9501	PBX9501	PBX9501
7	SFM [ft/min]	1220	976	610	610	488	366	244	122	122	61	61	30	350
8	Depth of cut [in]	0.125	0.125	0.125	0.125	0.125	0.125	0.125	0.125	0.125	0.125	0.125	0.125	0.125
9	Feed [in]	0.01	0.01	0.02	0.01	0.01	0.01	0.01	0.02	0.01	0.02	0.01	0.02	0.03
10	Diameter [in]	4.15	3.9	3.65	3.4	3.15	2.9	2.65	2.4	2.15	1.9	1.65	1.4	1.15
11	Length of cut [in]	3.73	3.73	3.73	3.73	3.73	3.73	3.73	3.73	3.73	3.73	3.73	3.73	3.73
12	rake angle α	0	0	0	0	0	0	0	0	0	0	0	0	0
13	Fx [N]	**-9.59**	**-10.24**	**-11.5**	**-9.45**	**-9.83**	**-10.49**	**-11.17**	**-12.99**	**-11.72**	**-11.04**	**-11.71**	**-9.09**	**N/A**
14	Fy [N]	**-5.92**	**-5.92**	**-9.77**	**-6.24**	**-6.57**	**-6.93**	**-7.21**	**-13.87**	**-9.12**	**-14.67**	**-9.72**	**-14.56**	**N/A**
15	Fz [N]	**36.45**	**37.16**	**66.08**	**37.04**	**38.4**	**38.75**	**39.1**	**61.51**	**39.1**	**55.23**	**35.94**	**44.86**	**N/A**
16	RPM	1123.47	956.39	638.69	685.65	592.05	482.32	351.88	194.27	216.86	122.70	141.29	81.89	1163.11
17	Fcut, Cutting force [N]	36.45	37.16	66.08	37.04	38.40	38.75	39.10	61.51	39.10	55.23	35.94	44.86	N/A
18	Ft, Thrust Force [N]	11.27	11.83	15.09	11.32	11.82	12.57	13.29	19.00	14.85	18.36	15.22	17.16	#VALUE!
19	Torque [N*m]	1.86	1.78	2.96	1.54	1.48	1.37	1.25	1.78	1.01	1.25	0.70	0.73	#VALUE!
20	friction coefficient	0.31	0.32	0.23	0.31	0.31	0.32	0.34	0.31	0.38	0.33	0.42	0.38	#VALUE!
21	(friction angle) β	17.19	17.67	12.87	17.01	17.12	17.98	18.79	17.18	20.81	18.40	22.96	20.95	#VALUE!
22	shear angle ϕ	36.41	36.17	38.57	36.50	36.44	36.01	35.61	36.41	34.60	35.80	33.52	34.53	#VALUE!
23	chip vel. Vc [m/s]	4.57	3.62	2.47	2.29	1.83	1.35	0.89	0.46	0.43	0.22	0.21	0.10	#VALUE!
24	shear vel. Vs [m/s]	7.70	6.14	3.96	3.85	3.08	2.30	1.52	0.77	0.75	0.38	0.37	0.18	#VALUE!
25	Cutting ratio r	0.74	0.73	0.80	0.74	0.74	0.73	0.72	0.74	0.69	0.72	0.66	0.69	#VALUE!
26	chip thickness tc [in]	0.17	0.17	0.16	0.17	0.17	0.17	0.17	0.17	0.18	0.17	0.19	0.18	#VALUE!

Figure 5.31. Experiment Parameters Fill Sheet Example Part 1 of 2

27	Resultant Force R [N]	38.15	39.00	67.78	38.73	40.18	40.74	41.30	64.38	41.83	58.20	39.03	48.03	#VALUE!
28	Shear plane Fs [N]	22.66	23.03	42.28	23.05	23.88	23.97	24.06	38.24	23.76	34.07	21.57	27.24	#VALUE!
29	Shear plane Fn [N]	30.70	31.47	52.98	31.13	32.31	32.94	33.57	51.79	34.42	47.19	32.53	39.56	#VALUE!
30	Tool-ship Forces F[N]	11.27	11.83	15.09	11.32	11.82	12.57	13.29	19.00	14.85	18.36	15.22	17.16	#VALUE!
31	P.shear [W]	174.43	141.40	167.51	88.83	73.57	55.07	36.67	29.44	17.89	13.01	8.02	5.04	#VALUE!
32	P.friction [W]	51.47	42.84	37.26	25.94	21.63	16.98	11.79	8.68	6.34	4.10	3.12	1.80	#VALUE!
33	P.shear+P.friction	225.90	184.24	204.77	114.78	95.20	72.05	48.47	38.12	24.23	17.11	11.14	6.84	#VALUE!
34	P.total calculated [W]	225.90	184.24	204.77	114.78	95.20	72.05	48.47	38.12	24.23	17.11	11.14	6.84	#VALUE!
35	P.total measured [W]	225.00	200.00	200.00	110.00	95.00	60.00	45.00	35.00	15.00	12.00	10.00	5.00	N/A
36	% shear	77%	77%	82%	77%	77%	76%	76%	77%	74%	76%	72%	74%	#VALUE!
37	% friction	23%	23%	18%	23%	23%	24%	24%	23%	26%	24%	28%	26%	#VALUE!
38	MRR [cm^3/sec]	5.00	4.00	5.00	2.50	2.00	1.50	1.00	1.00	0.50	0.50	0.25	0.25	4.30
39	shear u.s [mJ/mm^3]	34.90	35.37	33.52	35.55	36.80	36.73	36.69	29.46	35.80	26.04	32.08	20.50	#VALUE!
40	friction u.f [mJ/mm^3]	10.30	10.72	7.45	10.38	10.82	11.32	11.80	8.69	12.69	8.21	12.49	7.32	#VALUE!
41	total spec. energy u [mJ/mm^3	45.20	46.08	40.97	45.94	47.62	48.06	48.49	38.14	48.49	34.25	44.57	27.82	#VALUE!
42	ΔT1.measured [K]	**102.43**	**103.11**	**101.06**	**91.14**	**85.36**	**76.32**	**61.05**	**48.21**	**36.91**	**25.23**	**22.37**	**13.72**	**N/A**
43	ΔT2.measured [K]	**55.31**	**56.707**	**54.39**	**49.85**	**47.06**	**40.92**	**32.12**	**24.09**	**19.77**	**12.5**	**12.04**	**6.8**	**N/A**
44	ΔT.surface, derived [K]													
45	ΔT.predicted [K]	182.55	172.77	165.47	147.27	141.74	129.97	114.58	90.12	90.96	64.24	66.38	41.20	#VALUE!
46	Time per rotation [ms]	53.41	62.74	93.94	87.51	101.34	124.40	170.51	308.85	276.68	489.02	424.67	732.67	51.59
47	Comment 1	vacuum	vacuum	vacuum	vacuum	vacuum	vacuum	vacuum	vacuum	vacuum	vacuum	vacuum	vacuum	vacuum
48	Comment 2													
49	Comment 3													

Figure 5.32. Experiment Parameters Fill Sheet Example Part 2 of 2

AppendixB

5.2 Protocol HE Machining, Updated 5-7-2017

All work to be performed by trained personnel, with a minimum of two personnel required when working with HE.

Material Preparation:

1. Remove storage container(s) containing the HE billet from magazine (across the parking lot from main building)
2. Trained personnel hand carries container(s) to main building
3. Place container(s) on prep table (table covered with non-slip mat)
4. Remove billet(s), place on table
5. Glue Plexiglas round stock (4 to 5 inches in diameter, about 4 inches long) to smooth end of billet (Used Urethane Adhesive, high peel strength, e.g. Hardman D-50)
6. Secure glued fixture in an upright position in the day storage magazine, place 2 kg weight on top of fixture during the minimum of 2 hour curing time.

Material Testing:

1. Secure building (put up warning signs at the two access doors: Danger, No Entry, Energetic Materials Test)
2. Verify that machine is de-energized by checking main emergency stop located at control station.
3. Trained personnel hand carries one of the fixtures into blockhouse, secure the plexiglas end into chuck/clamp, leaving about 1 inch (machined step in plexiglas) between the end of the chuck/clamp and the HE billet.

4. Leave block house
5. Gather all personnel at control station (behind protective wall to the south end of block house)
6. Verify that all personnel are wearing ear and eye protection (2 personnel is minimum)
7. Energize machine
8. Run machining program
   (a) One remote lathing operator, zeroes tool settings through remote control, remote video observation, and runs automated machining profile
   (b) One additional observer, watching the operation remotely from camera feed inside block house
   (c) Both, operator and observer are ready to pull emergency stop
9. De-energize machine

Material Removal and Disposal:

1. Wait until machine is de-energized (end of machining) before entering the block house.
2. Both operator and observer agree that it is safe for operator to walk into block house.
3. Trained personnel removes leftover material from chuck or clamping device
4. Place fixture on prep table, remove Plexiglas end
5. Use brush and vacuum to gather machining dust, shavings; place residue in plastic bag
6. Add the leftover billet to plastic bag

7. Place plastic bag in day storage box
8. Go to Material Testing as needed
9. Carry day storage box with plastic bags and HE to outdoor disposal site
10. Place a maximum of two bags into disposal site (below ground burner system, remote operation)
11. Move away from disposal site and remotely ignite burners
12. Let cool off for a minimum 1 hour and verify temperature before reusing disposal site